JOURNAL OF GUIDANCE, CONTROL, AND DYNAMICS
Vol. 42, No. 7, July 2019

Finite-Time Estimation and Control for Multi-Aircraft Systems Under Wind and Dynamic Obstacles

Kunal Garg* and Dimitra Panagou†
University of Michigan, Ann Arbor, Michigan 48109

DOI: 10.2514/1.G003967

In this paper, the problem of generating safe trajectories for multi-agent systems in the presence of wind and dynamic obstacles is considered. A robust controller is designed to counteract a class of state disturbances that can be thought of as wind disturbance for aerial vehicles. The considered disturbance is unmatched, bounded with known bounds, with no assumptions on the regularity properties or the distribution of the disturbance. It is also assumed that only partial states are observed, and finite-time state-estimator-based finite-time state-feedback control is used to generate the system trajectories. It is shown that, even with limited and erroneous sensing, agents are capable of avoiding collisions with moving obstacles and with each other. The designed protocol is distributed, scalable with the number of agents, and of provable safety and convergence guarantees.

Nomenclature

$\boldsymbol{a}_i$	=	acceleration of agent i
d_{ij}	=	distance between agents i and j
$\hat{d}_{ij}$	=	estimated distance between agents i and j
d_m	=	minimum safety distance
$\boldsymbol{F}_i$	=	nominal vector field for agent i
R_s	=	sensing radius of each agent
$\mathbb{R}_+$	=	set of nonnegative reals
$\boldsymbol{r}_{\text{gi}}$	=	desired goal location of agent i
$\boldsymbol{r}_i$	=	position of agent i
$\hat{\boldsymbol{r}}_i$	=	estimated position of agent i
$\boldsymbol{r}^i_{\text{js}}$	=	position of agent j as sensed by agent i
$\boldsymbol{u}_i$	=	velocity of agent i
$\hat{\boldsymbol{u}}_i$	=	estimated velocity of agent i
u_{id}	=	desired speed for agent i
$\hat{\boldsymbol{u}}_{\text{id}}$	=	desired estimated velocity for agent i
$\boldsymbol{u}^i_{\text{js}}$	=	velocity of agent j as sensed by agent i
$\boldsymbol{w}$	=	wind disturbance
$\boldsymbol{w}_{\text{av}}$	=	mean value of the wind disturbance
γ_i	=	desired direction of motion for agent i
δ_{av}	=	variation of wind disturbance from mean value
δ_e	=	estimation error
ϵ_s	=	sensing error
$\|\cdot\|$	=	Euclidean norm (2-norm)
$\angle(\boldsymbol{x})$	=	orientation of vector $\boldsymbol{x}$
$\boldsymbol{0}$	=	zero vector
$\varnothing$	=	empty set

I. Introduction

A. Motivation

IN RECENT years, the usability of unmanned aerial vehicles (UAVs) has increased due to availability and technology maturity. This holds especially true for multirotor-type UAVs, which are now used for several commercial and consumer applications, such as package transportation [1] and distributed sensing [2], to name a few. Large-scale problems make centralized algorithms intractable with the number of agents, motivating the research in the field of distributed coordination and control. The problem of decentralized multi-agent motion planning, which mainly focuses on generating collision-free trajectories for multiple agents (e.g., UAVs) so that they reach preassigned goal locations under limited sensing, communication, and interaction capabilities, has been studied by many researchers in the past two decades; for recent overviews, the reader is referred to [3–5].

In this paper, we consider the problem of safe trajectory generation for multirotor-type UAVs for low-altitude urban environment operations. Specifically, we seek to generate safe trajectories from every initial condition to any goal location for vehicles modeled under double-integrator dynamics with limited, erroneous sensing capabilities, in the presence of unknown wind disturbance and moving obstacles while maintaining safety. Furthermore, we make use of finite-time stability theory so that the agents accomplish the assigned tasks in finite time.

B. Relevant Work

Numerous methodologies on distributed motion planning of multi-agent systems have appeared in recent years, with the most popular being 1) optimization-based techniques [6–8]; 2) Lyapunov-based methods, [9,10]; 3) Voronoi-diagram-based methods [11,12], and 4) graph search methods (for example A^* planning [13], Pareto optimization [14], and sampling-based methods, e.g., Rapidly-exploring random trees [15–17]); see also [18,19] for the overview of various path/motion planning algorithms. Lyapunov-based controllers are of particular interest for multi-agent problems because they are scalable with the number of agents and bring in the merits of Lyapunov-based analysis for safety and convergence guarantees.

Various methods using Lyapunov-like scalar functions have been employed for multi-agent motion planning problems, such as avoidance functions [20], potential functions [21], navigation functions [22,23], and harmonic functions [24]. The idea of directly defining vector fields as feedback motion plans is also well studied. Relevant work employing vector fields for vehicle navigation can be found in [25–27] and references therein. In [28,29], Rodrguez-Seda et al. consider the problem of collision avoidance for cooperative and noncooperative agents. However, they only consider the case of two vehicles, with complete knowledge of the state of the vehicle without any external disturbance.

The main issue with sampling-based or graph-based methods is scalability with number of agents. The scalability issues can be circumvented by using Lyapunov-based methods, such as navigation fields. One of the issues with using navigation fields and similar methods (e.g., potential functions) is the possible occurrence of deadlock points or surfaces, wherein the resultant vector field vanishes. In our earlier work [30], we only guaranteed almost global convergence due to the occurrence of deadlock for a set of initial

Received 23 July 2018; revision received 5 January 2019; accepted for publication 7 January 2019; published online 6 March 2019.

*Ph.D. Candidate, Department of Aerospace Engineering, 1320 Beal Avenue. Student Member AIAA.

†Assistant Professor, Department of Aerospace Engineering, 1320 Beal Avenue. Member AIAA.

conditions of measure zero. In this work, we address the problem of avoiding the deadlock by properly defining the direction of motion for the agents when the vector field vanishes, so that we have global convergence.

C. Limited and Erroneous Sensing

In the aforementioned work [20–30], it is assumed that each agent has perfect knowledge of its own states as well as of its neighbors' states. From practical and robustness point of view, sensing uncertainties along with the case when only partial state measurements are available should be considered. Another important aspect is the limited capabilities of the considered vehicles, in terms of limited sensing and communication radii. From the safety perspective, the agents must be able to avoid collisions with each other and with obstacles under these limitations. In [28], Rodrguez-Seda et al. consider limited sensing radius for a pair of nonholonomic vehicles for cooperative and noncooperative collision avoidance. In [23], Cheng et al. used potential functions for formation control and obstacle avoidance under limited sensing. In [31] (see also [32]), Ahn et al. design a centralized supervisor for collision avoidance in the presence of disturbances and uncontrolled vehicles. However, the work in [23,28,31,32] assumes complete knowledge of the states of the agents and no sensing uncertainties. In this work, we design a robust controller that guarantees safety and convergence when only partial state measurements are available, and there are sensing uncertainties in both the position and velocity of each agent.

D. Disturbance Modeling

Ensuring certain levels of robustness against modeling uncertainties and external disturbances is of primary concern for real-world applications. Much work is done for the case of matched disturbances (i.e., when the control input and the disturbance enter to the plant via the same channel). In [33], a stable uncertainty is assumed to be bounded in $\mathcal{H}_\infty$-norm by some prior given desired tolerance, and an observer-based controller is designed by using the algebraic Riccati equation. Related work considering bounded deterministic disturbances can be found in the design of finite-time consensus algorithms with matched disturbances [34–36], mismatched disturbances [37], and the rotating consensus control with mixed model uncertainties and external disturbances [38].

Wind, modeled as a state disturbance, affects the position trajectories of the aerial vehicles. For most of the practical systems, such as fixed-wing (or rotary-wing) aircraft, the control inputs are the deflection of control surfaces and thrust (or the rotor speed), which take effect in the velocity dynamics of the vehicle. Hence, the study of systems with unmatched disturbance becomes significantly important. Nevertheless, there is only little work in this field; in [39], Rezaei and Stefanovic assumed that the dynamics of the unmatched disturbance are known and leverage this knowledge to design a disturbance observer. In [40], Wang et al. assumed that the disturbance is an element of $\mathcal{L}_\infty$. Wang et al. [41] and Tian et al. [42] assumed that the disturbance satisfies a strong regularity condition that the disturbance should be at least twice differentiable for a second-order system, and all the derivatives of the disturbance are bounded with known bounds. Although under these strong assumptions, the aforementioned work showed that the effect of the disturbance can be nullified, it is worth noting that one cannot always assume such smoothness or vanishing properties for wind disturbances. In our earlier work [43,44], the wind disturbance was modeled as Gaussian disturbance with known mean and variance. We relax this assumption by allowing the wind to have any arbitrary distribution, which we do not assume to be known. Instead, we assume a general class of state disturbances that can vary both in space and time, and unlike [39–44], we assume that only the mean value and the maximum deviation of the disturbance from the mean value are known.

E. Finite-Time Stability in Multi-Agent Systems

It is often desired that the agents achieve their tasks of reaching given locations in a finite time. Also, for estimator-based full-state feedback, the convergence of estimation error in a finite time is desired. Finite-time stability (FTS) has been a well-studied concept, motivated in part from a practical viewpoint due to properties such as achieving convergence in finite time as well as exhibiting robustness with respect to disturbances [45]. The authors in [46] focus on continuous autonomous systems and present Lyapunov-like necessary and sufficient conditions for a system to exhibit FTS, whereas in [47], they provide geometric conditions for homogeneous systems to exhibit FTS. Finite-time controllers have been used for applications such as consensus or formation control in [48–50], but without any consideration of safety or collision avoidance. There is a large body of literature on collision avoidance schemes along with finite-time convergence, e.g., Li et al. [51,52] and Hu et al. [53] consider finite-time consensus with interagent collision avoidance, whereas Ma and Lai [54] incorporate collision avoidance in finite-time flocking of Cucker–Smale agents. Wang et al. [55] consider the problem of "parallel formation" (or velocity alignment) in a finite time in a stationary-obstacle environment. Although the aforementioned work considers interagent collision avoidance or obstacle avoidance, none of them consider any external disturbances or uncertainties in the state measurements. Zuo and Tie [56] consider bounded, matched disturbance and present a method of achieving robust finite-time consensus for multi-agent systems. Recent work, such as [35,36], considers bounded, matched disturbances, whereas Defoort et al. [57] consider unknown nonlinearities in the dynamics and design protocols to achieve consensus in a fixed time. However, the work in [35,36,56,57] does not consider any collision avoidance. In this paper, we consider finite-time convergence in the presence of external disturbances and sensor uncertainties, along with collision avoidance of the agents with each other and with dynamic obstacles.

F. Our Contributions

We consider the motion of class-A or controlled agents in a dynamic obstacle environment induced by class-B or uncontrolled agents (or simply dynamic obstacles), as defined in [30]. The dynamic obstacles do not cooperate toward collision avoidance. Compared to our earlier work in [30], where the agents were modeled as unicycles to capture the no-slip condition for carlike vehicles, here we model the agents under double-integrator dynamics for two-dimensional (2-D) motion of multirotor aircraft. In [30], perfect communication between the agents was assumed while each agent had knowledge of whether the neighboring agents are cooperative or noncooperative. In this paper, 1) the agents do not know whether their neighbors are cooperative or noncooperative, and 2) there is no active communication between the agents. We rather assume a limited sensing model that is erroneous (i.e., the agents can sense position and velocity of their neighboring agents but with some bounded error). Also, in contrast to [58] where the nominal, disturbance-free case was treated, we consider a general class of unmatched, state disturbances in the agents' dynamics to account for wind disturbances. Furthermore, in contrast to our prior work [30,58], in which all the states were assumed to be known, here we assume that only position measurements are available and make use of a state estimator for the control design of the agents. We design an FTS state-feedback control law that uses state estimates derived from an FTS state estimator. To the best of our knowledge, this is the first time that a finite-time estimator-based, finite-time feedback controller is used in the presence of disturbances and moving obstacles with safety considerations for multi-agent systems. Also, in contrast to any of the prior work of the authors, in which only almost global convergence was guaranteed, here we design a novel way of defining the desired direction of motion that eliminates the deadlock situation and guarantees global convergence.

In summary, the contributions of this paper are as follows.

1) We present a robust, distributed coordination protocol that accommodates for a class of unknown, bounded, unmatched disturbances in the agents' dynamics; the disturbance can have spatial as well as temporal variation.

2) We treat the case of dynamic obstacles with bounded speeds and prove safety of the system under sensing errors and external disturbances.

3) We consider limited, erroneous sensing and provide safety guarantees.

4) We make use of a state estimator-based feedback for the case when only partial state measurements are available.

5) We make use of finite-time stability theory for both state estimation and state-feedback control design for better performance, both in terms of convergence and disturbance rejection.

6) We use a novel desired direction of motion for the agents' planning and control so that provable safety and global convergence guarantees can be obtained.

7) Our proposed vector field method is distributed and is scalable with the number of agents.

G. Organization of the Paper

In Sec. II, we provide an overview of the modeling of the system under the effect of disturbances. We first present the vector field design for each agent i, which is by construction safe and convergent, and then design a state-feedback controller so that agents follow their respective vector fields in the nominal case (i.e., when there is no external disturbance and complete state information is available). In Sec. III, we present the robust observer-based control design. We first design a finite-time observer to reconstruct the state when only partial states are observed. Then, we design the robust controller using the estimated states and prove safety and convergence of the system. In Sec. IV, we treat the case of dynamic obstacles. Developing upon the controller from Sec. III, we design a safe protocol that assures collision avoidance with dynamic obstacles also. In Sec. V, we present the simulation results, and in Sec. VI, we discuss the performance of the designed protocol. Conclusions are summarized in Sec. VII.

II. Modeling and Problem Statement

Let us consider N identical agents $i \in \{1, \ldots, N\}$, which are assigned to move to goal locations of position coordinates $\boldsymbol{r}_{\mathrm{gi}} = [\,x_{\mathrm{gi}} \quad y_{\mathrm{gi}}\,]^T$ while avoiding collisions (i.e., for all agents $i \neq j$, $\|\boldsymbol{r}_i(t) - \boldsymbol{r}_j(t)\| \geq d_m$ for all $t \geq 0$, where d_m is a user-defined safety distance). Each agent i is assumed to be a multirotor aircraft whose equations of motion for 2-D planar motion can be approximated via double-integrator dynamics. In this paper, we restrict the motion of the agents to 2-D (or planar) motion. One of the main reasons for this constraint is that we are considering the problem of safe trajectory generation of the multirotor aircraft flying in low-altitude urban airfield with restrictions on the airspace available for such operations, particularly in terms of altitude restrictions. It is to be noted that, with anticipated increase in the number of vehicles in the airspace, it would be desired to have altitude bands designated to different classes of UAVs depending upon their capabilities. Thus, it is desired to design safe trajectories of the aircraft with fixed altitude constraints. Hence, we use the following dynamics to model the motion of the agents:

$$\dot{\boldsymbol{r}}_i(t) = \boldsymbol{u}_i(t) + \boldsymbol{w}(\boldsymbol{r}_i(t), t) \tag{1a}$$

$$\dot{\boldsymbol{u}}_i(t) = \boldsymbol{a}_i(t) \tag{1b}$$

$$\boldsymbol{y}_i(t) = \boldsymbol{r}_i(t) \tag{1c}$$

where $\boldsymbol{r}_i(t) = [\,x_i(t) \quad y_i(t)\,]^T$ is the position vector of the agent i, $\boldsymbol{y}_i(t)$ is the output map of the system consisting of the position of the agent i, $\boldsymbol{u}_i(t) = [\,u_{ix}(t) \quad u_{iy}(t)\,]^T$ is the velocity vector comprising the linear velocities of the agent i, and $\boldsymbol{a}_i(t) = [\,a_{ix}(t) \quad a_{iy}(t)\,]^T$ is the acceleration input to the agent i. The term $\boldsymbol{w}(\boldsymbol{r}_i, t)$:$\mathbb{R}^2 \times \mathbb{R}_+ \to \mathbb{R}^2$ is the wind disturbance, which can vary in both space and time. As can be seen from Eq. (1), the disturbance $\boldsymbol{w}(\boldsymbol{r}_i, t)$ is unmatched. We make the following assumption about the disturbance $\boldsymbol{w}(\boldsymbol{r}, t)$.

Assumption 1: The norm of the wind disturbance is bounded as

$$\|\boldsymbol{w}(\boldsymbol{r}, t) - \boldsymbol{w}_{\mathrm{av}}\| \leq \delta_w \quad \forall\ (\boldsymbol{r}, t) \in \mathcal{D} \subseteq \mathbb{R}^2 \times \mathbb{R}_+ \tag{2}$$

where

$$\boldsymbol{w}_{\mathrm{av}} = \frac{\int_{\mathcal{D}} \boldsymbol{w}(\boldsymbol{r}, t)\, \mathrm{d}\boldsymbol{s}}{\int_{\mathcal{D}} \mathrm{d}\boldsymbol{s}}$$

is the average or mean value of the disturbance with $\|\boldsymbol{w}_{\mathrm{av}}\| < \infty$, and $\delta_w < \infty$ is the maximum deviation of the disturbance from the mean value. Furthermore, the parameters $\boldsymbol{w}_{\mathrm{av}}$ and δ_w are known.

Remark 1: We only assume that the disturbance is bounded with known bound and known mean value. Our assumptions on the unmatched disturbance $\boldsymbol{w}(\boldsymbol{r}, t)$ are much less conservative as compared to the following literature.

1) In [39], Rezaei and Stefanovic assumed that the dynamics of the disturbance are known.

2) In [40], Wang et al. assumed that the disturbance is an element of $\mathcal{L}_\infty$.

3) In [41], Wang et al. assumed that the disturbance satisfies a stronger regularity assumption (i.e., it should be at least twice differentiable for double-integrator systems).

Each agent i has a circular sensing region $\mathcal{C}_i$ of radius R_c centered at $\boldsymbol{r}_i = [\,x_i \quad y_i\,]^T$, denoted as $\mathcal{C}_i$:$\{\boldsymbol{r} \in \mathbb{R}^2 | \|\boldsymbol{r}_i - \boldsymbol{r}\| \leq R_c\}$ We denote $\mathcal{N}_i = \{j | \boldsymbol{r}_j \in \mathcal{C}_i\}$ the set of agents that are in the sensing region of agent i and call them the neighboring agents (or simply neighbors) of agent i. Agent i can sense the position and velocity of any agent $j \in \mathcal{N}_i$. To this end, we make the following assumption on the sensing error for each agent i.

Assumption 2: Agent i can sense the position (denoted as $\boldsymbol{r}^i_{\mathrm{js}}$) and velocity (denoted as $\boldsymbol{u}^i_{\mathrm{js}}$) of any agent $j \in \mathcal{N}_i$ within a bounded error ϵ_s, i.e., $\|\boldsymbol{r}_j(t) - \boldsymbol{r}^i_{\mathrm{js}}(t)\| \leq \epsilon_s$ and $\|\boldsymbol{u}_j(t) - \boldsymbol{u}^i_{\mathrm{js}}(t)\| \leq \epsilon_s$.

Also, we make the following assumption on the initial and goal location of the agents and the sensing radius R_c to ensure safety and convergence.

Assumption 3: For each pair (i, j) such that $i \neq j$, $\|\boldsymbol{r}_i(0) - \boldsymbol{r}_j(0)\| > d_s$ and $\|\boldsymbol{r}_{\mathrm{gi}} - \boldsymbol{r}_{\mathrm{gj}}\| \geq 2R_c$, where d_s is the modified safety distance as defined in Theorem 5. Furthermore, the sensing radius satisfy $R_c > 2d_s$.

For each agent i, we design a vector field-based feedback controller. First, we design a vector field that can steer the agents toward their goal locations while maintaining safe interagent distances. Then, we design a feedback law to follow this vector field, as per our prior work in [30]. For the sake of brevity, the explicit dependence on time is dropped in the following sections.

A. Vector Field Design

We seek two categories of vector fields to achieve our objectives.

Attractive vector field: We use a radially attractive vector field that navigates agent i toward its goal location $\boldsymbol{r}_{\mathrm{gi}}$, given as

$$\boldsymbol{F}_{\mathrm{gi}} = -\frac{(\boldsymbol{r}_i - \boldsymbol{r}_{\mathrm{gi}})}{\|\boldsymbol{r}_i - \boldsymbol{r}_{\mathrm{gi}}\|} \tag{3}$$

Vector field (3) is globally attractive. This would ensure that, whenever agent i is conflict-free (i.e., $\mathcal{N}_i = \varnothing$), it moves toward its goal location. Note that, at $\boldsymbol{r}_i = \boldsymbol{r}_{\mathrm{gi}}$, the vector field $\boldsymbol{F}_{\mathrm{gi}}$ is defined to be $\boldsymbol{0}$ so that it is defined everywhere on $\mathbb{R}^2$.

Repulsive vector field: To maintain a safe distance from agent $j \in \mathcal{N}_i$, agent i operates under a radially repulsive field $\boldsymbol{F}_{ij}$ given by

$$\boldsymbol{F}_{ij} = \frac{\boldsymbol{r}_i - \boldsymbol{r}_j}{\|\boldsymbol{r}_i - \boldsymbol{r}_j\|} \tag{4}$$

This is a radially repulsive field, which would make agent i move away from any agent $j \in \mathcal{N}_i$

B. Blending Attractive and Repulsive Vector Fields

Let $d_{ij} = \|\boldsymbol{r}_i - \boldsymbol{r}_j\|$ be the interagent distance between agent i and j. Because we assume limited sensing radius R_c for agent i, and we need agent i maintains d_m as the minimum separation from all other

agents, we design the following bump function to blend the attractive and repulsive fields [30]. Define the function $\sigma_{ij}(\cdot):\mathbb{R}_+ \to [0,1]$:

$$\sigma_{ij}(d_{ij}) = \begin{cases} 1, & d_m \le d_{ij} < d_r; \\ ad_{ij}^3 + bd_{ij}^2 + cd_{ij} + d, & d_r \le d_{ij} \le R_c; \\ 0, & d_{ij} > R_c; \end{cases} \quad (5)$$

where d_r is a positive constant such that $d_m < d_r < R_c$. The coefficients a, b, c, d have been computed as

$$a = -\frac{2}{(d_r - R_c)^3}, \quad b = \frac{3(d_r + R_c)}{(d_r - R_c)^3},$$
$$c = -\frac{6d_r R_c}{(d_r - R_c)^3}, \quad d = \frac{R_c^2(3d_r - R_c)}{(d_r - R_c)^3}$$

so that the bump function σ_{ij} given as per Eq. (5) is a $\mathcal{C}^1$ function.

One may now define the vector field for each agent i as

$$\boldsymbol{F}_i = \sum_{j\in\mathcal{N}_i} \sigma_{ij}\boldsymbol{F}_{ij} + \prod_{j\in\mathcal{N}_i}(1-\sigma_{ij})\boldsymbol{F}_{\text{gi}} \quad (6)$$

The blending of the vector fields according to Eq. (6) means that, whenever agent i is far away from all the other agents (i.e., $d_{ij} > R_c$ for all j), only the globally attractive vector field is active, whereas if there are other agents in its vicinity, the net vector field is a weighted average of the attractive field $\boldsymbol{F}_{\text{gi}}$ and the repulsive field $\boldsymbol{F}_{ij}$. In the case when there is an agent j very close to agent i (i.e., $d_{ij} < d_r$), only the repulsive vector field $\boldsymbol{F}_{ij}$ is active.

The controller objective is to design a controller $\boldsymbol{a}_i$ for each agent i, so that the motion of each agent i is along the vector field F_i. We design the desired velocity $\boldsymbol{u}_{\text{id}}$ to be tracked with its direction $\angle\boldsymbol{u}_{\text{id}}$ along Eq. (6), and we design its magnitude $\|\boldsymbol{u}_{\text{id}}\|$ so that the safety is ensured at all times. The desired direction of motion of agent i is set to be

$$\gamma_i = \begin{cases} \tan^{-1}\left(\dfrac{\boldsymbol{F}_{iy}}{\boldsymbol{F}_{ix}}\right), & \|\boldsymbol{F}_i\| > 0; \\ \tan^{-1}\left(\dfrac{(x_i - x_{\text{gi}})}{-(y_i - y_{\text{gi}})}\right), & \|\boldsymbol{F}_i\| = 0 \end{cases} \quad (7)$$

Note that

$$\tan^{-1}\left(\frac{(x_i - x_{\text{gi}})}{-(y_i - y_{\text{gi}})}\right)$$

is the orientation of the vector perpendicular to the vector $\boldsymbol{r}_i - \boldsymbol{r}_{\text{gi}}$ pointing to its right. We define this desired direction for the case when $\|\boldsymbol{F}_i\| = 0$ so that there is no deadlock, as showed in the following lemma. Let

$$\gamma_i^0 \triangleq \tan^{-1}\left(\frac{(x_i - x_{\text{gi}})}{-(y_i - y_{\text{gi}})}\right)$$

Lemma 1: There is no deadlock (i.e., the agents would not get stuck) at any location other than their goal location $\boldsymbol{r}_{\text{gi}}$ for all times, if the direction of the motion of each agent i is along γ_i given by Eq. (7).

Proof: It is sufficient to prove that, if displaced along γ_i when $\boldsymbol{F}_i = \boldsymbol{0}$, the resulting field at the displaced location drives the agent away from the point of deadlock. More specifically, if $\boldsymbol{r}_i$ is the position of the agent i such that $\boldsymbol{F}_i(\boldsymbol{r}_i) = \boldsymbol{0}$, then after displacement $\delta\boldsymbol{r}_i$ along the direction γ_i, we need $\boldsymbol{F}_i(\boldsymbol{r}_i + \delta\boldsymbol{r}_i) \neq \boldsymbol{0}$, and $\angle\boldsymbol{F}_i(\boldsymbol{r}_i + \delta\boldsymbol{r}_i) = \gamma_i$, which results in agent i moving away from $\boldsymbol{r}_i$.

Let us consider a scenario with K agents, where $2 \le K \le N$, such that, for each agent i among these K agents, located at $\boldsymbol{r}_i$, the resulting vector fields $\boldsymbol{F}_i(\boldsymbol{r}_i) = \boldsymbol{0}$; an example is shown in Fig. 1. We can assume that, for all $j \in \mathcal{N}_i$, we have $\boldsymbol{F}_j = \boldsymbol{0}$. If this is not true for some j, then this agent would have a nonzero vector field along which it moves with a nonzero speed, and hence it would either go out of the sensing region of the agent i in a finite time, or it would reach a location $\boldsymbol{r}_j$ such that $\boldsymbol{F}_j(\boldsymbol{r}_j) = \boldsymbol{0}$.

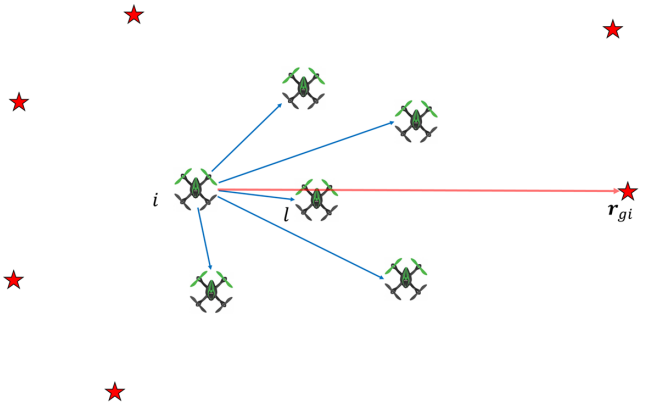

Fig. 1 Scenario with six agents located such that their resultant vector fields are 0. Blue arrows represent the vectors $\boldsymbol{r}_j - \boldsymbol{r}_i$ for each $j \in \mathcal{N}_i$, and the red arrow represents the vector $\boldsymbol{r}_{\text{gi}} - \boldsymbol{r}_i$.

We denote the effect of the rest of the $K-1$ agents on the agent i as a cumulative repulsive field $\boldsymbol{F}_{\text{rep}}$, so that we have

$$\boldsymbol{F}_i = \boldsymbol{F}_{\text{rep}} + \prod_{j\in\mathcal{N}_i}(1-\sigma_{ij})\boldsymbol{F}_{\text{gi}} = \boldsymbol{0} \quad (8)$$

Let

$$\bar{\sigma} = \prod_{j\in\mathcal{N}_i}(1-\sigma_{ij})$$

As per Fig. 1, there is at least one agent i such that $(\boldsymbol{r}_{\text{gi}} - \boldsymbol{r}_i)^T(\boldsymbol{r}_j - \boldsymbol{r}_i) \ge 0$ for all $j \in \mathcal{N}_i$ and at least one $l \in \mathcal{N}_i$ such that $(\boldsymbol{r}_{\text{gi}} - \boldsymbol{r}_i)^T(\boldsymbol{r}_l - \boldsymbol{r}_i) > 0$. This implies that $\boldsymbol{F}_{\text{gi}}^T\boldsymbol{F}_{\text{il}} < 0$ for at least one $l \in \mathcal{N}_i$ (or equivalently $\boldsymbol{F}_{\text{gi}}^T\boldsymbol{F}_{\text{rep}} < 0$) because $\boldsymbol{F}_{\text{il}}$ acts along $-(\boldsymbol{r}_l - \boldsymbol{r}_i)$. Using this, from Eq. (8), we have

$$\boldsymbol{F}_{\text{gi}}^T\boldsymbol{F}_i = \boldsymbol{F}_{\text{gi}}^T\boldsymbol{F}_{\text{rep}} + \bar{\sigma}\|\boldsymbol{F}_{\text{gi}}\|^2 = 0 \quad (9)$$

Because $\boldsymbol{F}_{\text{gi}}^T\boldsymbol{F}_{\text{rep}} < 0$, for Eq. (9) to hold, we need $\bar{\sigma} > 0$. Define an auxiliary agent o located at a location $\boldsymbol{r}_o$ to model the effect of the accumulated repulsive forces on agent i. Let the repulsive field of agent o on agent i be given by $\boldsymbol{F}_{io} = \boldsymbol{F}_{\text{rep}}/\bar{\sigma}$, and $\boldsymbol{r}_o$ is such that it satisfies

$$\frac{\boldsymbol{r}_i - \boldsymbol{r}_o}{\|\boldsymbol{r}_i - \boldsymbol{r}_o\|} = \frac{\boldsymbol{F}_{\text{rep}}}{\bar{\sigma}}$$

so that we have

$$\boldsymbol{F}_i(\boldsymbol{r}_i) = \boldsymbol{F}_{io} + \boldsymbol{F}_{\text{gi}} = \boldsymbol{0} \quad (10)$$

Equation (10) depicts a two-agent scenario consisting of agents i and o, such that $\boldsymbol{F}_l(\boldsymbol{r}_l) = \boldsymbol{0}$ for $l \in \{i, o\}$ (see Fig. 2). Because the direction of the motion of the agent i along γ_i^0 is perpendicular to the vector $\boldsymbol{r}_i - \boldsymbol{r}_{\text{gi}}$, let us denote it by the unit vector $(\boldsymbol{r}_i - \boldsymbol{r}_{\text{gi}})^\perp$. Hence, the displacement vector for agent i at the location $\boldsymbol{r}_i$ is given by $\delta\boldsymbol{r}_i = \delta_0(\boldsymbol{r}_i - \boldsymbol{r}_{\text{gi}})^\perp$, where $\delta_0 > 0$ denotes the infinitesimal length. Note that the resultant motion of the auxiliary agent o may or may not be perpendicular to $\boldsymbol{r}_i - \boldsymbol{r}_{\text{gi}}$ because it would depend upon the locations of the rest of the $K-1$ agents. Denote $\delta\boldsymbol{r}_o$ the displacement of the auxiliary agent o, so that it satisfies

$$\delta\boldsymbol{r}_o = -\delta_1(\boldsymbol{r}_i - \boldsymbol{r}_{\text{gi}})^\perp + \delta_2(\boldsymbol{r}_i - \boldsymbol{r}_{\text{gi}})^\parallel \quad (11)$$

where $(\boldsymbol{r}_i - \boldsymbol{r}_{\text{gi}})^\parallel$ denotes a unit vector along $(\boldsymbol{r}_i - \boldsymbol{r}_{\text{gi}})$, $\delta_1 > 0$, and δ_2 can be either positive or negative. This is true because the motion of

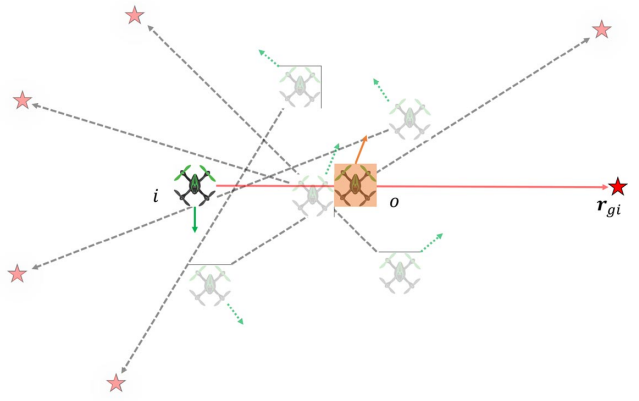

Fig. 2 Motion of the agents along γ_i^0. Gray arrows show the vector $r_{\text{gi}} - r_i$, green arrows show the direction of motion of agents along γ_i^0. The virtual agent is shown in orange.

the agent o would be in the opposite direction as agent i along the vector $(\boldsymbol{r}_i - \boldsymbol{r}_{\text{gi}})^{\perp}$ but can be in the either directions along the vector $(\boldsymbol{r}_i - \boldsymbol{r}_{\text{gi}})^{\parallel}$. Using this, we can express the vector field $\boldsymbol{F}_i$ after this infinitesimal displacement as

$$\begin{aligned}
&\boldsymbol{F}_i(\boldsymbol{r}_i + \delta\boldsymbol{r}_i, \boldsymbol{r}_o + \delta\boldsymbol{r}_o) = \boldsymbol{F}_{io}(\boldsymbol{r}_i + \delta\boldsymbol{r}_i, \boldsymbol{r}_o + \delta\boldsymbol{r}_o) + \boldsymbol{F}_{\text{gi}}(\boldsymbol{r}_i + \delta\boldsymbol{r}_i)\\
&= \left(\boldsymbol{F}_{io}(\boldsymbol{r}_i, \boldsymbol{r}_o) + \frac{\partial \boldsymbol{F}_{io}(\boldsymbol{r}_i, \boldsymbol{r}_o)}{\partial \boldsymbol{r}_i}\delta\boldsymbol{r}_i + \frac{\partial \boldsymbol{F}_{io}(\boldsymbol{r}_i, \boldsymbol{r}_o)}{\partial \boldsymbol{r}_o}\delta\boldsymbol{r}_o\right)\\
&+ \left(\boldsymbol{F}_{\text{gi}}(\boldsymbol{r}_i) + \frac{\partial \boldsymbol{F}_{\text{gi}}(\boldsymbol{r}_i)}{\partial \boldsymbol{r}_i}\delta\boldsymbol{r}_i\right)\\
&\overset{(10)}{=} \left(\frac{\partial \boldsymbol{F}_{io}(\boldsymbol{r}_i, \boldsymbol{r}_o)}{\partial \boldsymbol{r}_i}\delta\boldsymbol{r}_i + \frac{\partial \boldsymbol{F}_{io}(\boldsymbol{r}_i, \boldsymbol{r}_o)}{\partial \boldsymbol{r}_o}\delta\boldsymbol{r}_o\right) + \left(\frac{\partial \boldsymbol{F}_{\text{gi}}(\boldsymbol{r}_i)}{\partial \boldsymbol{r}_i}\delta\boldsymbol{r}_i\right)\\
&\overset{(11)}{=} \left(\frac{\partial \boldsymbol{F}_{io}(\boldsymbol{r}_i, \boldsymbol{r}_o)}{\partial \boldsymbol{r}_i}\delta_0(\boldsymbol{r}_i - \boldsymbol{r}_{\text{gi}})^{\perp} + \frac{\partial \boldsymbol{F}_{io}(\boldsymbol{r}_i, \boldsymbol{r}_o)}{\partial \boldsymbol{r}_o}\left(-\delta_1(\boldsymbol{r}_i - \boldsymbol{r}_{\text{gi}})^{\perp}\right.\right.\\
&\left.\left. + \delta_2(\boldsymbol{r}_i - \boldsymbol{r}_{\text{gi}})^{\parallel}\right)\right) + \left(\frac{\partial \boldsymbol{F}_{\text{gi}}(\boldsymbol{r}_i)}{\partial \boldsymbol{r}_i}\delta_0(\boldsymbol{r}_i - \boldsymbol{r}_{\text{gi}})^{\perp}\right)\\
&\overset{(3),(4)}{=} \left(\frac{\boldsymbol{I}d_{io}^2 - \boldsymbol{r}_{oi}\boldsymbol{r}_{oi}^T}{d_{io}^3}\delta_0(\boldsymbol{r}_i - \boldsymbol{r}_{\text{gi}})^{\perp} - \frac{\boldsymbol{I}d_{io}^2 - \boldsymbol{r}_{oi}\boldsymbol{r}_{oi}^T}{d_{io}^3}\left(-\delta_1(\boldsymbol{r}_i - \boldsymbol{r}_{\text{gi}})^{\perp}\right.\right.\\
&\left.\left. + \delta_2(\boldsymbol{r}_i - \boldsymbol{r}_{\text{gi}})^{\parallel}\right)\right) + \left(\frac{-\boldsymbol{I}d_{\text{gi}}^2 + (\boldsymbol{r}_i - \boldsymbol{r}_{\text{gi}})(\boldsymbol{r}_i - \boldsymbol{r}_{\text{gi}})^T}{d_{\text{gi}}^3}\delta_0(\boldsymbol{r}_i - \boldsymbol{r}_{\text{gi}})^{\perp}\right)
\end{aligned}$$

where $d_{\text{gi}} = \|\boldsymbol{r}_i - \boldsymbol{r}_{\text{gi}}\|$, $\boldsymbol{r}_{oi} = \boldsymbol{r}_i - \boldsymbol{r}_o$, and $\boldsymbol{I} \in \mathbb{R}^{2\times 2}$ is the identity matrix. Note that $\boldsymbol{r}_{oi}$ is also along $(\boldsymbol{r}_i - \boldsymbol{r}_{\text{gi}})^{\parallel}$, and hence it is perpendicular to $(\boldsymbol{r}_i - \boldsymbol{r}_{\text{gi}})^{\perp}$. Using this, we obtain

$$\begin{aligned}
\boldsymbol{F}_i(\boldsymbol{r}_i + \delta\boldsymbol{r}_i, \boldsymbol{r}_o + \delta\boldsymbol{r}_o) &= \left(\frac{\delta_0(\boldsymbol{r}_i - \boldsymbol{r}_{\text{gi}})^{\perp}}{d_{io}} + \frac{\delta_1(\boldsymbol{r}_i - \boldsymbol{r}_{\text{gi}})^{\perp}}{d_{io}}\right.\\
&\left. - \frac{\boldsymbol{I}d_{io}^2 - \boldsymbol{r}_{oi}\boldsymbol{r}_{oi}^T}{d_{io}^3}\left(\delta_2(\boldsymbol{r}_i - \boldsymbol{r}_{\text{gi}})^{\parallel}\right)\right) + \frac{-\delta_0(\boldsymbol{r}_i - \boldsymbol{r}_{\text{gi}})^{\perp}}{d_{\text{gi}}}\\
&= \left(\frac{\delta_0(\boldsymbol{r}_i - \boldsymbol{r}_{\text{gi}})^{\perp}}{d_{io}} + \frac{\delta_1(\boldsymbol{r}_i - \boldsymbol{r}_{\text{gi}})^{\perp}}{d_{io}} - \frac{\delta_0(\boldsymbol{r}_i - \boldsymbol{r}_{\text{gi}})^{\perp}}{d_{\text{gi}}}\right.\\
&\left. - \frac{\boldsymbol{I}d_{io}^2 - \boldsymbol{r}_{oi}\boldsymbol{r}_{oi}^T}{d_{io}^3}\left(\delta_2(\boldsymbol{r}_i - \boldsymbol{r}_{\text{gi}})^{\parallel}\right)\right)
\end{aligned}$$

Also note that $(\boldsymbol{I}d_{io}^2 - \boldsymbol{r}_{oi}\boldsymbol{r}_{oi}^T)\delta_2(\boldsymbol{r}_i - \boldsymbol{r}_{\text{gi}})^{\parallel} = \delta_2 d_{io}^2(\boldsymbol{r}_i - \boldsymbol{r}_{\text{gi}})^{\parallel} - \delta_2\boldsymbol{r}_{oi}\boldsymbol{r}_{oi}^T(\boldsymbol{r}_i - \boldsymbol{r}_{\text{gi}})^{\parallel} = \boldsymbol{0}$ for all $\boldsymbol{r}_{oi}$. Hence, for $\boldsymbol{F}_i(\boldsymbol{r}_i + \delta\boldsymbol{r}_i, \boldsymbol{r}_o + \delta\boldsymbol{r}_o) = \boldsymbol{0}$ to hold, we need

$$\frac{\delta_0 + \delta_1}{d_{io}} = \frac{\delta_0}{d_{\text{gi}}}$$

Hence, it is needed that

$$d_{\text{gi}} = \frac{\delta_0}{\delta_0 + \delta_1}d_{io} < d_{io}$$

Because agent o is in the sensing radius of agent i, we obtain $d_{\text{gi}} < d_{io} < R_c$. Using the same set of arguments as before for some other agent j from the rest of the $K-1$ agents, we can obtain $d_{gj} < d_{jo'} < R_c$, where o' is the auxiliary agent corresponding to agent j. Because the repulsive forces for agents i and j cancel out the attractive fields toward their respective goal location, we obtain that their goal locations $\boldsymbol{r}_{\text{gi}}$ and $\boldsymbol{r}_{\text{gj}}$ are located toward their front, using which we obtain $\|\boldsymbol{r}_{\text{gi}} - \boldsymbol{r}_{\text{gj}}\| \le R_c$, which violates Assumption 3. Hence, if the goal locations are chosen as per Assumption 3, the condition

$$d_{\text{gi}} = \frac{\delta_0}{\delta_0 + \delta_1}d_{io}$$

would never hold, and hence we have that $\boldsymbol{F}_i(\boldsymbol{r}_i + \delta\boldsymbol{r}_i, \boldsymbol{r}_o + \delta\boldsymbol{r}_o) \neq \boldsymbol{0}$. Furthermore, we note that, from Assumption 3, there is at least one agent i out of the K agents such that $d_{\text{gi}} > d_{ij}$, which implies that $\boldsymbol{F}_i(\boldsymbol{r}_i + \delta\boldsymbol{r}_i, \boldsymbol{r}_o + \delta\boldsymbol{r}_o)$ is along $(\boldsymbol{r}_i - \boldsymbol{r}_{\text{gi}})^{\perp}$, making agent i move away from the position $\boldsymbol{r}_i$ for which $\boldsymbol{F}_i(\boldsymbol{r}_i) = 0$, which completes the proof. □

We first design a desired velocity command with magnitude u_{id} and direction $\boldsymbol{u}_{\text{id}n} = [\cos\gamma_i \quad \sin\gamma_i]^T$ for each agent i, which tracks the vector field [Eq. (6)], so that the trajectories of the agent i are collision-free and reach the goal location $\boldsymbol{r}_{\text{gi}}$. We then consider the error between the actual velocity $\boldsymbol{u}_i$ and the desired linear velocity $\boldsymbol{u}_{\text{id}}$ of agent i, and we design an acceleration controller $\boldsymbol{a}_i$ that drives this error to zero in finite time. We ensure that the safety is maintained by enlarging the safety distance d_m by the maximum transient error induced by the velocity error $\boldsymbol{u}_i - \boldsymbol{u}_{\text{id}}$.

C. State Feedback Design

To design the desired velocity command $\boldsymbol{u}_{\text{id}}$ that generates collision-free position trajectories for kinematic subsystem (1a) of each agent i, we build upon the control design in [9]. In our prior work [58], the desired velocity vector is defined as $\boldsymbol{u}_{\text{id}} = u_{\text{id}}\boldsymbol{u}_{\text{id}n}$, where $\boldsymbol{u}_{\text{id}n} = [\cos\gamma_i \quad \sin\gamma_i]^T$, and u_{id} of agent i is set as

$$u_{\text{id}} = \begin{cases} \frac{1}{\mu}\log\left(\left(\sum_{j\in\mathcal{N}_i|J_i<0} e^{-\mu u_{i|j}}\right)^{-1} + 1\right), & d_m \le d_{ij} \le R_c;\\ u_{\text{ic}}, & d_{ij} > R_c; \end{cases} \tag{12}$$

where $u_{i|j}$ denotes the velocity adjustment mechanism of agent i with respect to agent j, defined as

$$u_{i|j} = u_{\text{ic}}\frac{d_{ij} - d_m}{R_c - d_m} + \varepsilon_i u_{\text{is}|j}\frac{R_c - d_{ij}}{R_c - d_m} \tag{13}$$

with the terms in Eq. (13) defined as

$$u_{\text{ic}}(\boldsymbol{r}_i) = \begin{cases} k_{i1}\tanh(\|\boldsymbol{r}_i - \boldsymbol{r}_{\text{gi}}\|), & \|\boldsymbol{r}_i - \boldsymbol{r}_{\text{gi}}\| > R_1;\\ k_{i2}\|\boldsymbol{r}_i - \boldsymbol{r}_{\text{gi}}\|^{\alpha_r}, & \|\boldsymbol{r}_i - \boldsymbol{r}_{\text{gi}}\| \le R_1; \end{cases} \tag{14a}$$

$$u_{\text{is}|j} = u_{\text{jd}}\frac{\boldsymbol{r}_{ji}^T\boldsymbol{u}_{\text{id}n}}{\boldsymbol{r}_{ji}^T\boldsymbol{u}_{\text{id}n}}, \quad J_i = \boldsymbol{r}_{ji}^T\boldsymbol{u}_{\text{id}n} \tag{14b}$$

where $0 < \alpha_r,\ \varepsilon_i < 1$, $\boldsymbol{r}_{ji} \triangleq \boldsymbol{r}_i - \boldsymbol{r}_j$, and $\mu \gg 1$ is a large positive number. Note that the term u_{ic} given in Eq. (14a) is defined differently from [30,58], so that we can guarantee finite-time convergence, unlike the prior work, in which only asymptotic convergence was guaranteed. Gains k_{i1}, k_{i2} and parameter R_1 are chosen such that u_{ic} is continuously differentiable for all $\boldsymbol{r}_i$. Hence, enforcing continuity of u_{ic} and its derivative when $\|\boldsymbol{r}_i - \boldsymbol{r}_{\text{gi}}\| = R_1$, we have

$$k_{i1}\tanh R_1 = k_{i2}R_1^{\alpha_r}; \quad k_{i1}(1-\tanh^2 R_1) = \alpha_r k_{i2}R_1^{\alpha_r-1} \tag{15}$$

From the preceding equations, we obtain R_1 as the solution of

$$(1-\tanh^2 R_1) = \alpha_r \frac{\tanh(R_1)}{R_1} \tag{16}$$

The preceding expression has a unique positive solution R_1 for any $0<\alpha_r<1$. For a given positive gain $k_{i1}>0$, k_{i2} is given as

$$k_{i2} = k_{i1}\frac{\tanh R_1}{R_1^{\alpha_r}}$$

The term $\|\boldsymbol{r}_i - \boldsymbol{r}_{\text{gi}}\|^{\alpha_r}$ ensures finite-time convergence (Theorem 6). We use Eq. (14a) so that the magnitude of the desired speed u_{ic} is bounded for all $\boldsymbol{r}_i$.

Remark 2: The expression given in Eq. (12) is a smooth approximation of the following function:

$$\max\left\{0, \min_{k\in\mathcal{N}_i|J_k<0} u_{i|k}\right\}$$

We first approximate the min function by

$$g(a) = -\frac{1}{\mu}\log\left(\sum_i e^{-\mu a_i}\right)$$

with $\mu \gg 1$, where $a = [\,a_1 \quad a_2 \quad \ldots, a_l\,]$. Using the smooth approximation for max function,

$$h(b) = \frac{1}{\mu}\log\left(\sum_i e^{\mu b_i}\right)$$

for $b = [\,g(a) \quad 0\,]$, we have that $h(b) = (1/\mu)\log(e^{\mu g(a)}+1)$. Using the fact that

$$e^{\mu g(a)} = e^{-\log\left(\sum_i e^{-\mu a_i}\right)} = \left(\sum_i e^{-\mu a_i}\right)^{-1}$$

we obtain the expression as in Eq. (12).

Remark 3: Note that the desired velocity in Eq. (12) assumes that agent i has perfect knowledge of its neighbor j's position and velocity. We relax this assumption in the robust control design (Sec. III). Also, we do not use the protocol defined in Eq. (12) directly, but we built upon it for the case of robust controller design. We write Eq. (12) here, directly from [30], for the sake of completeness.

With this desired velocity in hand, the acceleration command can be chosen as

$$\boldsymbol{a}_i = \dot{\boldsymbol{u}}_{\text{id}} - \lambda_i(\boldsymbol{u}_i - \boldsymbol{u}_{\text{id}})\|\boldsymbol{u}_i - \boldsymbol{u}_{\text{id}}\|^{\alpha-1} \tag{17}$$

where $\lambda_i>0$, and $0<\alpha<1$, so that the velocity error $\boldsymbol{u}_i - \boldsymbol{u}_{\text{id}}$ converges to $\boldsymbol{0}$ in finite time.[‡] Because in this paper, we assume that only the position of agent i is measured, we first design a state estimator to be able to implement a full-state feedback. Then, we redesign the desired velocity command (denoted as $\hat{\boldsymbol{u}}_{\text{id}}$) for the estimator dynamics so that it is robust with respect to the state disturbance $\boldsymbol{w}(\boldsymbol{r},t)$ and sensing uncertainties.

III. Robust Control Design

A. Overview of Finite-Time Stability

We first define the notion of finite-time stability and present some related results.

[‡]This can be verified using $\boldsymbol{x} = \boldsymbol{u}_i - \boldsymbol{u}_{\text{id}}$ in Theorem 3.

Definition 1 [46]: The origin for the system $\dot{\boldsymbol{x}}(t) = \boldsymbol{f}(\boldsymbol{x}(t))$ is called an FTS equilibrium (or simply FTS) if, in some domain $\mathcal{D}\subseteq\mathbb{R}^n$ containing the origin, it is stable in the sense of Lyapunov, and it is finite-time converging (i.e., there exists a finite time T), such that $\lim_{t\to T}\boldsymbol{x}(t) = \boldsymbol{0}$. Furthermore, if these conditions hold globally (i.e., $\mathcal{D}=\mathbb{R}^n$), then the origin is called globally FTS equilibrium (or simply globally FTS).

Theorem 1 [46]: The origin for the system $\dot{\boldsymbol{x}}(t) = \boldsymbol{f}(\boldsymbol{x}(t))$ is FTS if there exists a positive-definite function $V(\boldsymbol{x}):\mathcal{D}\to\mathbb{R}$, such that it satisfies $\dot{V}(\boldsymbol{x}) + cV(\boldsymbol{x})^{\alpha} \le 0$ along the system trajectories for some $c>0$, $0<\alpha<1$ for all $\boldsymbol{x}\in\mathcal{V}\setminus\{\boldsymbol{0}\}$, where $\mathcal{V}\subseteq\mathcal{D}$ is an open neighborhood of the origin. If $\mathcal{D}=\mathbb{R}^n$, V is proper, and $\dot{V}$ takes negative values for all $\boldsymbol{x}\in\mathbb{R}^n\setminus\{\boldsymbol{0}\}$, then the origin is globally FTS.

Definition 2 [47]: A function $\boldsymbol{f}:\mathbb{R}^n\to\mathbb{R}^n$ is called a homogeneous function with degree d with respect to a dilation function $\Delta_\epsilon(\boldsymbol{x}) = (\epsilon^{r_1}x_1, \epsilon^{r_2}x_2, \ldots, \epsilon^{r_n}x_n)$, where $r_i>0$ and $\boldsymbol{x} = [\,x_1 \quad x_2 \quad \ldots \quad x_n\,]^T$, if for each i, $f_i(\epsilon^{r_1}x_1, \epsilon^{r_2}x_2, \ldots, \epsilon^{r_n}x_n) = \epsilon^{d+r_i}f_i(x_1, x_2, \ldots, x_n)$ for any $\epsilon>0$.

Theorem 2 [47]: Suppose that the vector field $\boldsymbol{f}$ is homogeneous with degree d. Then, the origin of the system $\dot{\boldsymbol{x}}(t) = \boldsymbol{f}(\boldsymbol{x}(t))$ is FTS if and only if it is asymptotically stable and $d<0$.

Theorem 3 [59]: The origin of the system $\dot{\boldsymbol{x}}(t) = -k\boldsymbol{x}\|\boldsymbol{x}\|^{\alpha-1}$ is globally FTS for any $k>0$ and $0<\alpha<1$.

B. Finite-Time Stable State Estimator

Feedback control law (17) requires full-state information. Because only partial state is available via system output, we make use of an FTS state estimator inspired from [60], given by

$$\dot{\hat{\boldsymbol{r}}}_i = \hat{\boldsymbol{u}}_i + k_{i3}(\boldsymbol{y}_i - \hat{\boldsymbol{y}}_i)\|\boldsymbol{y}_i - \hat{\boldsymbol{y}}_i\|^{\alpha_1-1} + \boldsymbol{w}_{\text{av}} \tag{18a}$$

$$\dot{\hat{\boldsymbol{u}}}_i = \boldsymbol{a}_i + k_{i4}(\boldsymbol{y}_i - \hat{\boldsymbol{y}}_i)\|\boldsymbol{y}_i - \hat{\boldsymbol{y}}_i\|^{\alpha_2-1} \tag{18b}$$

where $\hat{\boldsymbol{y}}_i = \hat{\boldsymbol{r}}_i$ is the estimated output, $0<\alpha_1,\ \alpha_2<1$, and k_{i3}, $k_{i4}>0$. Define the error terms $\boldsymbol{r}_{\text{ie}} \triangleq \boldsymbol{r}_i - \hat{\boldsymbol{r}}_i = \boldsymbol{y}_i - \hat{\boldsymbol{y}}_i$ and $\boldsymbol{u}_{\text{ie}} \triangleq \boldsymbol{u}_i - \hat{\boldsymbol{u}}_i$ so that, from Eqs. (1) and (18), we obtain

$$\dot{\boldsymbol{r}}_{\text{ie}} = \boldsymbol{u}_{\text{ie}} - k_{i3}\boldsymbol{r}_{\text{ie}}\|\boldsymbol{r}_{\text{ie}}\|^{\alpha_1-1} + \boldsymbol{w}(\boldsymbol{r}_i,t) - \boldsymbol{w}_{\text{av}} \tag{19a}$$

$$\dot{\boldsymbol{u}}_{\text{ie}} = -k_{i4}\boldsymbol{r}_{\text{ie}}\|\boldsymbol{r}_{\text{ie}}\|^{\alpha_2-1} \tag{19b}$$

To show the finite-time convergence of the estimation error, we first need the following results.

Lemma 2: If $\boldsymbol{w}(\boldsymbol{r}_i,t) = \boldsymbol{0}$, the origin is an asymptotically stable equilibrium of system (19).

Proof: Note that $\boldsymbol{w}(\boldsymbol{r}_i,t) = \boldsymbol{0}$ implies that there is no external disturbance. Choose the candidate Lyapunov function:

$$V(\boldsymbol{r}_{\text{ie}},\boldsymbol{u}_{\text{ie}}) = \frac{k_{i4}}{1+\alpha_2}\|\boldsymbol{r}_{\text{ie}}\|^{1+\alpha_2} + \frac{1}{2}\|\boldsymbol{u}_{\text{ie}}\|^2$$

Taking its time derivative along the trajectories of Eq. (19), we obtain

$$\dot{V}(\boldsymbol{r}_{\text{ie}},\boldsymbol{u}_{\text{ie}}) = k_{i4}\|\boldsymbol{r}_{\text{ie}}\|^{\alpha_2-1}\boldsymbol{r}_{\text{ie}}^T\left(\boldsymbol{u}_{\text{ie}} - k_{i3}\boldsymbol{r}_{\text{ie}}\|\boldsymbol{r}_{\text{ie}}\|^{\alpha_1-1}\right) + \boldsymbol{u}_{\text{ie}}^T\left(-k_{i4}\boldsymbol{r}_{\text{ie}}\|\boldsymbol{r}_{\text{ie}}\|^{\alpha_2-1}\right) = -k_{i3}k_{i4}\|\boldsymbol{r}_{\text{ie}}\|^{\alpha_1+\alpha_2} \le 0$$

Now, because $\alpha_1+\alpha_2>0$, $\dot{V}(\boldsymbol{r}_{\text{ie}},\boldsymbol{u}_{\text{ie}}) = 0$ at $\boldsymbol{r}_{\text{ie}}\equiv\boldsymbol{0}$ for any $\boldsymbol{u}_{\text{ie}}$. Using LaSalle's invariance principle, we have that the origin is the only point where the trajectories of system (19) can identically stay. Hence, the origin is an asymptotically stable equilibrium for system (19) when $\boldsymbol{w}(\boldsymbol{r}_i,t) = \boldsymbol{0}$. □

Lemma 3: For $\boldsymbol{w}(\boldsymbol{r}_i,t) = \boldsymbol{0}$ and $\alpha_1 = \alpha$, $\alpha_2 = 2\alpha - 1$, where $(1/2)<\alpha<1$, the error dynamics [Eq. (19)] is homogeneous with degree of homogeneity $d = \alpha - 1 < 0$.

Proof: Let $r_1 = 1$ and $r_2 = \alpha$, with $(1/2)<\alpha<1$. With these parameters, define the dilation function $\Delta_\epsilon(\boldsymbol{r},\boldsymbol{u}) = (\epsilon\boldsymbol{r}, \epsilon^{\alpha}\boldsymbol{u})$. Define

the right-hand side of Eq. (19) as $\boldsymbol{f}^{\text{err}}(\boldsymbol{r}_{\text{ie}}, \boldsymbol{u}_{\text{ie}}) = [\, f_1^{\text{err}}(\boldsymbol{r}_{\text{ie}}, \boldsymbol{u}_{\text{ie}}) \quad f_2^{\text{err}}(\boldsymbol{r}_{\text{ie}}, \boldsymbol{u}_{\text{ie}}) \,]^T$. Now, for $\boldsymbol{w}(\boldsymbol{r}_i, t) = \boldsymbol{0}$, define $d \triangleq \alpha - 1$ so that, for any $\epsilon > 0$, we obtain

$$\begin{aligned} f_1^{\text{err}}\left(\epsilon^{r_1}\boldsymbol{r}_{\text{ie}}, \epsilon^{r_2}\boldsymbol{u}_{\text{ie}}\right) &= \epsilon^{r_2}\boldsymbol{u}_e - k_{i3}\epsilon^{r_1\alpha_1}\boldsymbol{r}_{\text{ie}}\|\boldsymbol{r}_{\text{ie}}\|^{\alpha_1-1} \\ &= \epsilon^{\alpha}\left(\boldsymbol{u}_e - k_{i3}\boldsymbol{r}_{\text{ie}}\|\boldsymbol{r}_{\text{ie}}\|^{\alpha_1-1}\right) \\ &= \epsilon^{d+r_1} f_1^{\text{err}}\left(\epsilon^{r_1}\boldsymbol{r}_{\text{ie}}, \epsilon^{r_2}\boldsymbol{u}_{\text{ie}}\right), \\ f_2^{\text{err}}\left(\epsilon^{r_1}\boldsymbol{r}_{\text{ie}}, \epsilon^{r_2}\boldsymbol{u}_{\text{ie}}\right) &= -k_{i4}\epsilon^{r_1\alpha_2} r_e \|\boldsymbol{r}_{\text{ie}}\|^{\alpha_2-1} \\ &= \epsilon^{2\alpha-1}\left(-k_{i4}\epsilon^{\boldsymbol{r}_1\alpha_2} r_e \|\boldsymbol{r}_{\text{ie}}\|^{\alpha_2-1}\right) \\ &= \epsilon^{d+r_2} f_2^{\text{err}}\left(\epsilon^{r_1}\boldsymbol{r}_{\text{ie}}, \epsilon^{r_2}\boldsymbol{u}_{\text{ie}}\right) \end{aligned}$$

Thus, from Definition 2, the error dynamics is homogeneous with degree $d = \alpha - 1 < 0$. □

From [47] (Theorem 7.1), we have that the origin is a finite-time stable equilibrium for Eq. (19) if $\boldsymbol{w}(\boldsymbol{r}_i, t) = \boldsymbol{0}$ (i.e., in the absence of the disturbance). Now, we show that, in the presence of the disturbance $\boldsymbol{w}(\boldsymbol{r}_i, t)$, the estimation error remains bounded.

Theorem 4: With α_1, α_2 as per Lemma 3, the norm of the state-estimation error is bounded as

$$\left\| [\, \boldsymbol{r}_{\text{ie}}(t)^T \quad \boldsymbol{u}_{\text{ie}}(t)^T \,]^T \right\| \le \delta_{\text{ie}}(t)$$

for all $t \ge 0$, where $\delta_{\text{ie}}(t)$ is defined as

$$\delta_{\text{ie}}(t) = \begin{cases} \|\boldsymbol{u}_{\text{ie}}(0)\|, & 0 \le t \le T_i^{\text{obs}}; \\ l_i \delta_w^{c_i}, & t > T_i^{\text{obs}}; \end{cases} \tag{20}$$

where $l_i = (2(1-\beta))^{(1-\beta)/\beta}\|\boldsymbol{u}_{\text{ie}}(0)\| > 0$, $c_i = (1-\beta)/\beta > 1$, $0 < \beta < (1/2)$, and $0 \le T_i^{\text{obs}} < \infty$ is a finite constant.

Proof: Define $z(t) = [\, \boldsymbol{r}_{\text{ie}}(t)^T \quad \boldsymbol{u}_{\text{ie}}(t)^T \,]^T$. First, note the nominal error dynamics, i.e., when the disturbance $\boldsymbol{w}(\boldsymbol{r}_i, t) = 0$, the origin is finite-time stable for system (19). Using [47] (Theorems 4.1, 6.2), we have that there exists a function $T(\boldsymbol{r}_{\text{ie}}, \boldsymbol{u}_{\text{ie}})$ that is continuous at the origin. Now, using this function as the settling time, from [46] (Theorem 4.3), we have that there exists a continuous Lyapunov function $V(\boldsymbol{r}_{\text{ie}}, \boldsymbol{u}_{\text{ie}})$ satisfying the condition $\dot{V}(\boldsymbol{r}_{\text{ie}}, \boldsymbol{u}_{\text{ie}}) + c(V(\boldsymbol{r}_{\text{ie}}, \boldsymbol{u}_{\text{ie}}))^{\beta} \le 0$, for some $c > 0$ and $0 < \beta < 1$ (namely, $V(\boldsymbol{r}_{\text{ie}}, \boldsymbol{u}_{\text{ie}}) = (T(\boldsymbol{r}_{\text{ie}}, \boldsymbol{u}_{\text{ie}}))^{1/(1-\beta)}$). Let β satisfy $\beta \in (0, 1/2)$. Because $\|\boldsymbol{w}(\boldsymbol{r}_i, t) - \boldsymbol{w}_{\text{av}}\| \le \delta_w$, using [46] (Theorem 5.2), we obtain that, with $z(0) \in \mathcal{U}$, where $\mathcal{U}$ is an open neighborhood of origin, $z(t) \in \mathcal{U}$ for all time $t \ge 0$. Define $\mathcal{U} = \{z \,|\, \|z\| \le \|z(0)\|\}$, so that $z(0) \in \mathcal{U}$. Because we can choose $\hat{\boldsymbol{r}}_i(0) = \boldsymbol{r}_i(0)$, we have that $\|z(t)\| \le \|z(0)\| = \|\boldsymbol{u}_{\text{ie}}(0)\|$. From this, we have that $\|z(t)\| \le \|\boldsymbol{u}_{\text{ie}}(0)\|$ for all time $t \ge 0$. Furthermore, again as per [46] (Theorem 5.2), there exists a finite time T_i^{obs} such that, for all $t \ge T_i^{\text{obs}}$,

$$\|z(t)\| \le l_i \delta_w^{c_i} \tag{21}$$

where $l_i = ((2(1-\beta))^{(1-\beta)/\beta}\|\boldsymbol{u}_{\text{ie}}(0)\| > 0$, $c_i = (1-\beta)/\beta > 1$. Hence, with choice of $\delta_{\text{ie}}(t)$ as per Eq. (20), we obtain that $\|z(t)\| \le \delta_{\text{ie}}(t)$ for all $t \ge 0$. □

Remark 4: The reason for using a finite-time state estimator instead of a Luenberger observer is that, as shown in [46], the bound on state (in our case, state-estimation error) δ_{ie} in Theorem 4 is of higher order than the bound on the disturbance δ_w ($c_i > 1$), leading to improved rejection of low-level persistent disturbances.

Next, we design a robust controller using the estimated states $\hat{\boldsymbol{r}}_i, \hat{\boldsymbol{u}}_i$.

C. Observer-Based Robust Controller

We first redesign the desired velocity using the estimated states as follows:

$$\hat{\boldsymbol{u}}_{\text{id}} = \hat{u}_{\text{id}}\hat{\boldsymbol{u}}_{\text{id}n} - k_{i3}\boldsymbol{r}_{\text{ie}}\|\boldsymbol{r}_{\text{ie}}\|^{\alpha_1-1} - \boldsymbol{w}_{\text{av}} \tag{22a}$$

$$\hat{\boldsymbol{u}}_{\text{id}n} = [\, \cos\hat{\gamma}_i \quad \sin\hat{\gamma}_i \,]^T \tag{22b}$$

where $\hat{\gamma}_i \triangleq \gamma_i(\hat{\boldsymbol{r}}_i)$. Note that, in the absence of actual state measurements, the vector field $\boldsymbol{F}_i$, $\hat{\gamma}_i$ and the bump function $\sigma = \sigma(\hat{d}_{ij})$, where $\hat{d}_{ij}$ is given by Eq. (26), are functions of the estimated/sensed positions. Define the set I_i as

$$I_i = \left\{ j \in \mathcal{N}_i \,|\, \hat{J}_i < 0, d_s \le \hat{d}_{ij} \le R_c \right\} \tag{23}$$

as the set of agents who are in the sensing range of agent i such that the agent i is moving toward them (i.e., $\hat{J}_i \triangleq \hat{\boldsymbol{r}}_{ji}^T\hat{\boldsymbol{u}}_{\text{id}n} < 0$). The new desired speed $\hat{u}_{\text{id}}$ for agent i is set as

$$\hat{u}_{\text{id}} = \begin{cases} \dfrac{1}{\mu}\log\left(\left(\sum_{j\in\mathcal{N}_i|\hat{d}_{ij}\le d_s} e^{-\mu\hat{u}_{\text{is}|j}}\right)^{-1} + 1\right), & I_i = \varnothing \;\&\; \hat{d}_{ij} \le d_s; \\ u_{\text{ic}}, & I_i = \varnothing \;\&\; \hat{d}_{ij} > d_s; \\ \dfrac{1}{\mu}\log\left(\left(\sum_{j\in I_i} e^{-\mu\hat{u}_{i|j}}\right)^{-1} + 1\right), & I_i \ne \varnothing \end{cases} \tag{24}$$

where $\hat{u}_{i|j}$ is defined as

$$\hat{u}_{i|j} = u_{\text{ic}}\frac{\hat{d}_{ij} - d_s}{R_c - d_s} + \hat{u}_{\text{is}|j}\frac{R_c - \hat{d}_{ij}}{R_c - d_s} \tag{25}$$

where d_s is defined as per Theorem 5, $u_{\text{ic}} = u_{\text{ic}}(\hat{\boldsymbol{r}}_i)$ is as per Eq. (14a), and the rest of the terms in Eq. (25) are given as

$$\begin{aligned} \hat{u}_{\text{is}|j} &= \varepsilon_i \frac{\hat{\boldsymbol{r}}_{ji}^T\boldsymbol{u}_{\text{js}}^i}{\hat{\boldsymbol{r}}_{ji}^T\hat{\boldsymbol{u}}_{\text{id}n}} + (1-\varepsilon_i)\frac{u_e d_s}{\hat{\boldsymbol{r}}_{ji}^T\hat{\boldsymbol{u}}_{\text{id}n}}, \quad 0 < \varepsilon_i < 1, \\ \hat{J}_j &= \hat{\boldsymbol{r}}_{ji}^T\hat{\boldsymbol{u}}_{\text{id}n}, \quad \hat{\boldsymbol{r}}_{ji} = \hat{\boldsymbol{r}}_i - \boldsymbol{r}_{\text{js}}^i, \quad \hat{d}_{ij} = \|\hat{\boldsymbol{r}}_{ji}\| \end{aligned} \tag{26}$$

where $\boldsymbol{u}_{\text{js}}^i$ and $\boldsymbol{r}_{\text{js}}^i$ are the position and velocity of agent $j \in \mathcal{N}_i$ as sensed by agent i, and u_e is defined later as per Eq. (31). Consider the dynamics [Eq. (18)] with an objective of tracking the velocity command $\hat{\boldsymbol{u}}_{\text{id}}$ given as per Eq. (32). We design the acceleration controller as follows:

$$\boldsymbol{a}_i = \dot{\hat{\boldsymbol{u}}}_{\text{id}} - \lambda_i\boldsymbol{u}_{\text{ide}}\|\boldsymbol{u}_{\text{ide}}\|^{\beta_2-1} - k_{i4}\boldsymbol{r}_{\text{ie}}\|\boldsymbol{r}_{\text{ie}}\|^{\alpha_2-1} \tag{27a}$$

$$\boldsymbol{u}_{\text{ide}} = \hat{\boldsymbol{u}}_i - \hat{\boldsymbol{u}}_{\text{id}} \tag{27b}$$

where $\lambda_i > 0$, $0 < \beta_2 < 1$, and $\boldsymbol{u}_{\text{ide}}$ is the velocity error between the desired velocity $\hat{\boldsymbol{u}}_{\text{id}}$ and the velocity of the observer $\hat{\boldsymbol{u}}_i$. In the next subsections, we show that system (1) converges to a small neighborhood of the desired goal location $\boldsymbol{r}_{\text{gi}}$ while maintaining safety.

D. Safety Analysis

First, we define the estimation error parameter δ_e as

$$\delta_e \triangleq \max_{i,t}\delta_{\text{ie}}(t) = \max_i\{\boldsymbol{u}_{\text{ie}}(0), l_i\delta_w^{c_i}\} \tag{28}$$

so that $\|\boldsymbol{r}_i(t) - \hat{\boldsymbol{r}}_i(t)\| \le \delta_e$ and $\|\boldsymbol{u}_i(t) - \hat{\boldsymbol{u}}_i(t)\| \le \delta_e$ for all agents i and for all time $t \ge 0$.

Theorem 5: Assume that N agents $i \in \{1, 2, \ldots, N\}$ are moving under the effect of acceleration controller (27). If the safe separation of each agent i is taken as $d_s = d_m + r_e + \delta_e + \epsilon_s$, with r_e being the maximum overshoot of the position error in the transient period of closed-loop system (18) given out of Eq. (36), and δ_e is defined as in Eq. (28), then the motion of all agents is collision-free (i.e., $\|\boldsymbol{r}_i(t) - \boldsymbol{r}_j(t)\| \ge d_m$ for all $i \ne j$ and for all $t \ge 0$).

Proof: Before we prove the safety, we note that the following inequality holds for all $t \ge 0$ and for all $i \ne j$:

$$\hat{d}_{ij} = \|\hat{\boldsymbol{r}}_i - \boldsymbol{r}^i_{\text{js}}\| \le \|\hat{\boldsymbol{r}}_i - \boldsymbol{r}_i\| + \|\boldsymbol{r}^i_{\text{js}} - \boldsymbol{r}_j\| + \|\boldsymbol{r}_i - \boldsymbol{r}_j\| \le \delta_e + \epsilon_s + \|\boldsymbol{r}_i - \boldsymbol{r}_j\|$$

which means that, if $\hat{d}_{ij} = \|\hat{\boldsymbol{r}}_i - \boldsymbol{r}^i_{\text{js}}\| \ge d_m + \epsilon_s + \delta_e$, then $d_{ij} = \|\boldsymbol{r}_i - \boldsymbol{r}_j\| \ge d_m$. Hence, we need to prove that $\hat{d}_{ij} \ge d_m + \epsilon_s + \delta_e$ holds for all time $t \ge 0$. From Assumption 3, we have that the interagent distance $d_{ij}(0) \ge d_m$, which means that all the agents start from a safe distance. Let j be some agent in the sensing region of the agent i at some time instant $t \ge 0$ (i.e., $\hat{d}_{ij}(t) \le R_c$). Denote the steady-state values of $\hat{\boldsymbol{r}}_i$ and $\hat{\boldsymbol{u}}_i$ as $\hat{\boldsymbol{r}}^{\text{ss}}_i$ and $\hat{\boldsymbol{u}}^{\text{ss}}_i$, respectively. Note that the steady-state velocity satisfies $\hat{\boldsymbol{u}}^{\text{ss}}_i = \boldsymbol{u}_{\text{id}}$. Consider the time derivative of the estimated distance, which in the steady state (i.e., when $\hat{\boldsymbol{u}}_i = \hat{\boldsymbol{u}}_{\text{id}}$ and $\hat{\boldsymbol{r}}_i = \hat{\boldsymbol{r}}^{\text{ss}}_i$) reads

$$\dot{\hat{d}}_{\text{ij}} = \frac{\hat{u}_{\text{id}}(\hat{\boldsymbol{r}}^{\text{ss}}_i - \boldsymbol{r}^i_{\text{js}})^T\hat{\boldsymbol{u}}_{\text{id}n} - (\hat{\boldsymbol{r}}^{\text{ss}}_i - \boldsymbol{r}^i_{\text{js}})^T\boldsymbol{u}^i_{\text{js}}}{\hat{d}^{\text{ss}}_{\text{ij}}} \tag{29}$$

The worst-case neighbor is the agent $j \in \{\mathcal{N}_i | \hat{J}_i < 0\}$ toward whom the rate of change of the estimated distance $\hat{d}_{ij}$ given by Eq. (29), due to the motion of agent i, is maximum. More specifically, the term $\hat{J}_i < 0$ describes the set of agents $j \in \mathcal{N}_i$ toward whom agent i is moving in its current direction (see [9] for more details). Consider the worst case (i.e., $\hat{d}^{\text{ss}}_{\text{ij}} = \|\hat{\boldsymbol{r}}^{\text{ss}}_i - \boldsymbol{r}^i_{\text{js}}\| = d_s$). The commanded speed $\hat{u}_{\text{id}}$ in this case is equal to $\hat{u}_{\text{is}|j}$, which is given as per Eq. (26). Plugging this into Eq. (29), we obtain

$$\dot{\hat{d}}_{ij} = \frac{(1-\varepsilon_i)u_e d_s + (\varepsilon_i - 1)(\hat{\boldsymbol{r}}_i - \boldsymbol{r}^i_{\text{js}})^T\boldsymbol{u}^i_{\text{js}}}{d_s} \tag{30}$$

Note that

$$\begin{aligned}(\hat{\boldsymbol{r}}_i - \boldsymbol{r}^i_{\text{js}})^T\boldsymbol{u}^i_{\text{js}} &= (\hat{\boldsymbol{r}}_i - \hat{\boldsymbol{r}}_j)^T\boldsymbol{u}^i_{\text{js}} + (\hat{\boldsymbol{r}}_j - \hat{\boldsymbol{r}}_{\text{js}})^T\boldsymbol{u}^i_{\text{js}} \\ &= (\hat{\boldsymbol{r}}_i - \hat{\boldsymbol{r}}_j)^T\hat{\boldsymbol{u}}_j + (\hat{\boldsymbol{r}}_i - \hat{\boldsymbol{r}}_j)^T(\boldsymbol{u}^i_{\text{js}} - \hat{\boldsymbol{u}}_j) + (\hat{\boldsymbol{r}}_j - \hat{\boldsymbol{r}}_{\text{js}})^T\boldsymbol{u}^i_{\text{js}}\end{aligned}$$

Using the fact that agent j either is moving away from agent i at the first place or is following the vector field that points away from agent i, we have $(\hat{\boldsymbol{r}}_i - \hat{\boldsymbol{r}}_j)^T\hat{\boldsymbol{u}}_j \le 0$ (where $\hat{\boldsymbol{u}}_j$ is the estimated velocity of agent j, available only to agent j). Furthermore, using the bounds on the estimation and sensing errors, we obtain

$$\begin{aligned}&(\hat{\boldsymbol{r}}_i - \hat{\boldsymbol{r}}_j)^T\hat{\boldsymbol{u}}_j + (\hat{\boldsymbol{r}}_i - \hat{\boldsymbol{r}}_j)^T(\boldsymbol{u}^i_{\text{js}} - \hat{\boldsymbol{u}}_j) + (\hat{\boldsymbol{r}}_j - \hat{\boldsymbol{r}}_{\text{js}})^T\boldsymbol{u}^i_{\text{js}} \\ &\quad\le (d_s + \epsilon_s)(\delta_e + \epsilon_s) + \epsilon_s\|\boldsymbol{u}^i_{\text{js}}\|\end{aligned}$$

Choose u_e as

$$u_e = \frac{(d_s + \epsilon_s)(\delta_e + \epsilon_s) + \epsilon_s\|\boldsymbol{u}^i_{\text{js}}\|}{d_s} \tag{31}$$

Now, from Eq. (30) and choice of u_e as per Eq. (31), we have

$$\begin{aligned}&(1-\varepsilon_i)u_e d_s + (\varepsilon_i - 1)(\hat{\boldsymbol{r}}_i - \boldsymbol{r}^i_{\text{js}})^T\boldsymbol{u}^i_{\text{js}} \\ &\quad\ge (1-\varepsilon_i)u_e d_s - (1-\varepsilon_i)\Big((d_s + \epsilon_s)(\delta_e + \epsilon_s) + \epsilon_s\|\boldsymbol{u}^i_{\text{js}}\|\Big) \ge 0\end{aligned}$$

This implies that the steady-state estimated interagent distance $\hat{d}^{\text{ss}}_{ij}$ cannot become less than d_s. Now, to account for the transient period, let us consider time derivative of the velocity error $\hat{\boldsymbol{u}}_{\text{ide}}$, which reads

$$\dot{\boldsymbol{u}}_{\text{ide}} = \dot{\hat{\boldsymbol{u}}}_i - \dot{\hat{\boldsymbol{u}}}_{\text{id}} = \boldsymbol{a}_i + k_{i4}\boldsymbol{r}_{\text{ie}}\|\boldsymbol{r}_{\text{ie}}\|^{\alpha_2 - 1} - \dot{\hat{\boldsymbol{u}}}_{\text{id}} \tag{32}$$

Substituting Eq. (27) into Eq. (32) yields

$$\dot{\boldsymbol{u}}_{\text{ide}} = -\lambda_i(\hat{\boldsymbol{u}}_i - \hat{\boldsymbol{u}}_{\text{id}})\|\hat{\boldsymbol{u}}_i - \hat{\boldsymbol{u}}_{\text{id}}\|^{\beta_2 - 1} = -\lambda_i\boldsymbol{u}_{\text{ide}}\|\boldsymbol{u}_{\text{ide}}\|^{\beta_2 - 1} \tag{33}$$

where $\lambda_i > 0$. From Theorem 3, we obtain that the origin is a finite-time stable equilibrium of system (33). Integrating Eq. (33) furthermore yields

$$\boldsymbol{u}_{\text{ide}}(t) = \boldsymbol{u}_{\text{ide}}(0)\left(1 - \frac{\lambda_i t(1-\beta_2)}{\|\boldsymbol{u}_{\text{ide}}(0)\|^{1-\beta_2}}\right)^{1/(1-\beta_2)} = c_1(1 - c_2 t)^{\xi} \tag{34}$$

where $\boldsymbol{u}_{\text{ide}}(0)$ is the initial velocity error, $c_1 = \boldsymbol{u}_{\text{ide}}(0)$,

$$c_2 = \frac{\lambda_i(1-\beta_2)}{\|\boldsymbol{u}_{\text{ide}}(0)\|^{1-\beta_2}}$$

and $\xi = 1/(1-\beta_2)$. Note that $\boldsymbol{u}_{\text{ide}}(t) = 0$ for all $t \ge t^* = (1/c_2)$. Hence, after this instant, the error in position would not change. By integrating Eq. (34), we obtain the transient position error $\boldsymbol{r}_{\text{ide}}(t)$ as

$$\boldsymbol{r}_{\text{ide}}(t) = \boldsymbol{r}_{\text{ide}}(0) + \frac{c_1}{c_2(1+\xi)}(1 - (1 - c_2 t)^{1+\xi}) \tag{35}$$

With $\boldsymbol{r}_{\text{ide}}(0) = 0$, we have that the maximum position error $\boldsymbol{r}_{\text{ieMax}}$, attained at $t^* = (1/c_2)$, has the form

$$\boldsymbol{r}_{\text{ieMax}} = \boldsymbol{r}_{\text{ide}}\left(\frac{1}{c_2}\right) = \frac{c_1}{c_2(1+\xi)} = \frac{\boldsymbol{u}_{\text{ide}}(0)\|\boldsymbol{u}_{\text{ide}}(0)\|^{1-\beta_2}}{\lambda_i(2-\beta_2)}$$

where $\boldsymbol{u}_{\text{ide}}(0) = \hat{\boldsymbol{u}}_i(0) - u_{\text{id}}(0)\boldsymbol{u}_{\text{id}n}(0) + \boldsymbol{w}_{\text{av}} + k_{i3}\boldsymbol{r}_{\text{ie}}(0)\|\boldsymbol{r}_{\text{ie}}(0)\|^{\alpha_1 - 1}$. Define r_e as

$$r_e = \max_i \|\boldsymbol{r}_{\text{ieMax}}\| \tag{36}$$

Note that, from the steady-state analysis, we have that $\|\hat{\boldsymbol{r}}^{\text{ss}}_i - \hat{\boldsymbol{r}}_{\text{js}}\| \ge d_s$. Using this, we obtain

$$\hat{d}_{ij} = \|\hat{\boldsymbol{r}}_i - \hat{\boldsymbol{r}}_{\text{js}}\| \ge \|\hat{\boldsymbol{r}}^{\text{ss}}_i - \hat{\boldsymbol{r}}_{\text{js}}\| - \|\hat{\boldsymbol{r}}_i - \hat{\boldsymbol{r}}^{\text{ss}}_i\| \ge d_s - r_e$$

Thus, with $d_s = d_m + \delta_e + \epsilon_s + r_e$, we have that $\hat{d}_{ij} \ge d_m + \delta_e + \epsilon_s$, and hence $d_{ij} \ge d_m$ (i.e., the resulting agent trajectories are collision-free).

E. Convergence Analysis

Now we show that, under the effect of the designed control law [Eq. (27)], the closed-loop trajectories of agent i reach the δ_{ie} neighborhood around the goal location $\boldsymbol{r}_{\text{gi}}$ in finite time. We need the following result before we proceed with the main result:

Lemma 4: Consider the system

$$\dot{\boldsymbol{x}}(t) = -k\boldsymbol{x}(t)\frac{\tanh(\|\boldsymbol{x}(t)\|)}{\|\boldsymbol{x}(t)\|}$$

for some $k > 0$. Assume that $\boldsymbol{x}(0) \ne \boldsymbol{0}$. Then, for any $\epsilon > 0$, there exists a time $T_\epsilon < \infty$ such that $\|\boldsymbol{x}(t)\| \le \epsilon$ for all $t \ge T_\epsilon$.

Proof: Let $V(\boldsymbol{x}) = (1/2)\|\boldsymbol{x}(t)\|^2$ be the candidate Lyapunov function. Taking the time derivative of $V(\boldsymbol{x})$ along the system trajectories, we obtain

$$\dot{V}(\boldsymbol{x}) = \boldsymbol{x}(t)^T\left(-k\boldsymbol{x}(t)\frac{\tanh\|\boldsymbol{x}(t)\|}{\|\boldsymbol{x}(t)\|}\right) = -k\|\boldsymbol{x}(t)\|\tanh(\|\boldsymbol{x}(t)\|)$$

This shows that $\dot{V}(\boldsymbol{x}(t)) < 0$ for all $\boldsymbol{x}(t) \ne \boldsymbol{0}$. Hence, we have that $V(\boldsymbol{x}(t)) \le V(\boldsymbol{x}(0))$ or $\|\boldsymbol{x}(t)\| \le \|\boldsymbol{x}(0)\|$ for all $t \ge 0$. Define $x_0 \triangleq \|\boldsymbol{x}(0)\|$ so that we have $\|\boldsymbol{x}(t)\| \le x_0$, and because $\boldsymbol{x}(0) \ne \boldsymbol{0}$, $x_0 > 0$. It is easy to check that the system trajectories satisfy

$$\tanh(\|\boldsymbol{x}(t)\|) \ge \frac{\tanh(x_0)}{x_0}\|\boldsymbol{x}(t)\|$$

for all $t \ge 0$ (i.e., the graph of $\tanh(\|\boldsymbol{x}(t)\|)$ lies above the straight line $y = c\|\boldsymbol{x}(t)\|$ with slope $c = \tanh(x_0)/x_0$ for all $\|\boldsymbol{x}(t)\| \le x_0$). Hence, we have that

$$\dot{V}(\boldsymbol{x}) = -k\|\boldsymbol{x}(t)\|\tanh(\|\boldsymbol{x}(t)\|) \leq -\frac{k\tanh(x_0)}{x_0}\|\boldsymbol{x}(t)\|^2 = -cV(\boldsymbol{x})$$

where

$$c = \frac{2k\tanh(x_0)}{x_0}$$

From the comparison lemma [61], we obtain $V(\boldsymbol{x}(t)) \leq e^{-ct}V(\boldsymbol{x}(0))$.

For a given $\epsilon > 0$, define

$$T_\epsilon = -\frac{1}{c}\log\left(\frac{\epsilon^2}{2V(\boldsymbol{x}(0))}\right)$$

so that we have $V(\boldsymbol{x}(T_\epsilon)) \leq e^{-cT\epsilon}V(\boldsymbol{x}(0)) = (1/2)\epsilon^2$. Now, because $V(\boldsymbol{x}(t)) \leq V(\boldsymbol{x}(T_\epsilon))$ for all $t \geq T_\epsilon$, we obtain $V(\boldsymbol{x}(t)) \leq (1/2)\epsilon^2$ or $\|\boldsymbol{x}(t)\| \leq \epsilon$ for all $t \geq T_\epsilon$. Also, because $\|\boldsymbol{x}_0\| \neq 0$, we have $T_\epsilon < \infty$. □

Now, we are ready to state the main result for convergence.

Theorem 6: Under the effect of control law (27), the closed-loop trajectories of Eq. (1) for each agent i reach the δ_{ie} neighborhood around the goal location $\boldsymbol{r}_{\text{gi}}$ in finite time (i.e., $\exists T_i < \infty$), such that $\|\boldsymbol{r}_i(t) - \boldsymbol{r}_{\text{gi}}\| \leq \delta_{\text{ie}}(t)$ for all time $t \geq T_i$.

Proof: From Lemma 1, we have that there is no deadlock, so that the agents are always attracted to their desired goal locations. The agents are following vector field (6) under the desired direction of motion given by Eq. (7), which takes each agent i away from the other agents and toward its goal location (i.e., each class-A agent resolves the conflict with all other agents). Also, from Assumption 3, we have that, once all agents reach their respective goal locations, they are out of each others' sensing region. Hence, once all the agents reach their respective goal locations, they stay there.

Now, we are ready to show that, once agent i resolves all its conflicts with the other agents, it would reach its goal location in finite time. Consider the error dynamics for $\hat{\boldsymbol{u}}_{\text{ide}}$, which, as per Eq. (33), reads $\dot{\hat{\boldsymbol{u}}}_{\text{ide}} = -\lambda_i(\boldsymbol{u}_{\text{ide}})\|\boldsymbol{u}_{\text{ide}}\|^{\beta_2 - 1}$. From Theorem 3, we have that the origin of system (33) is finite-time stable. This implies that there exists a time t_i such that, for all $t \geq t_i$, $\hat{\boldsymbol{u}}_i(t) = \boldsymbol{u}_{\text{id}}(t)$. Note that, from Eqs. (22) and (18), we obtain $\dot{\hat{\boldsymbol{r}}}_i(t) = \hat{u}_{\text{id}}\hat{\boldsymbol{u}}_{\text{id}n}$ for all $t \geq t_i$. Now, in the absence of any neighbors, from Eq. (22), we have that $\hat{u}_{\text{id}} = \hat{u}_{\text{ic}}$, and the direction of vector field $\hat{\boldsymbol{u}}_{\text{id}n}$ is along $\boldsymbol{F}_i(\hat{\boldsymbol{r}}_i) = \boldsymbol{F}_{\text{gi}}(\hat{\boldsymbol{r}}_i)$, i.e., along $-(\hat{\boldsymbol{r}}_i - \boldsymbol{r}_{\text{gi}})$. Hence, the dynamics of the desired trajectory $\hat{\boldsymbol{r}}_{\text{id}}$ reads

$$\dot{\hat{\boldsymbol{r}}}_i = -\hat{u}_{\text{ic}}\frac{(\hat{\boldsymbol{r}}_i - \boldsymbol{r}_{\text{gi}})}{\|\hat{\boldsymbol{r}}_i - \boldsymbol{r}_{\text{gi}}\|} \tag{37}$$

Now, if at the instant when error $\hat{\boldsymbol{u}}_{\text{ide}}(t)$ becomes $\boldsymbol{0}$, the value of the norm $\|\hat{\boldsymbol{r}}_i - \boldsymbol{r}_{\text{gi}}\| \leq R_1$, then $\hat{u}_{\text{ic}}$ in Eq. (37) directly takes the form $\hat{u}_{\text{ic}} = k_{i2}\|\hat{\boldsymbol{r}}_i - \boldsymbol{r}_{\text{gi}}\|^{\alpha_r}$. If this is not the case, then, by Lemma 4, we obtain that there exists a finite time $\tilde{t}_i$, after which $\|\hat{\boldsymbol{r}}_i - \boldsymbol{r}_{\text{gi}}\|$ is less than R_1. Now, after this point, the value $\hat{u}_{\text{ic}}$ as per Eq. (14a) reads $\hat{u}_{\text{ic}} = k_{i2}\|\hat{\boldsymbol{r}}_i - \boldsymbol{r}_{\text{gi}}\|^{\alpha_r}$; hence, we obtain

$$\dot{\hat{\boldsymbol{r}}}_i = -k_{i2}\|\hat{\boldsymbol{r}}_i - \boldsymbol{r}_{\text{gi}}\|^{\alpha_r}\frac{(\hat{\boldsymbol{r}}_i - \boldsymbol{r}_{\text{gi}})}{\|\hat{\boldsymbol{r}}_i - \boldsymbol{r}_{\text{gi}}\|} = -k_{i2}(\hat{\boldsymbol{r}}_i - \boldsymbol{r}_{\text{gi}})\|\hat{\boldsymbol{r}}_i - \boldsymbol{r}_{\text{gi}}\|^{\alpha_r - 1} \tag{38}$$

From Theorem 3, we have that $\boldsymbol{r}_{\text{gi}}$ is a finite-time stable equilibrium for Eq. (38). Hence, we obtain that there exists some finite time T_i^*, such that, for all $t \geq T_i^*$, $\hat{\boldsymbol{r}}_i = \boldsymbol{r}_{\text{gi}}$. Now, from Theorem 4, we have that $\|\boldsymbol{r}_i(t) - \hat{\boldsymbol{r}}_i(t)\| \leq \delta_{\text{ie}}(t)$ for all $t \geq T_i^{\text{obs}}$. Define $T_i = \max\{T_i^*, T_i^{\text{obs}}\} < \infty$, and so we obtain that, for all $t \geq T_i$, $\|\boldsymbol{r}_i(t) - \hat{\boldsymbol{r}}_i(t)\| = \|\boldsymbol{r}_i(t) - \boldsymbol{r}_{\text{gi}}\| \leq \delta_{\text{ie}}(t)$, which completes the proof. □

IV. Dynamic Obstacle Environment

Let us now consider the case when the agents, termed as class-A agents subsequently, have to navigate in the obstacle environment. We consider M dynamic obstacles $o \in \mathcal{N}_B = \{N+1, \ldots, N+M\}$, which are moving with upper-bounded linear velocity $\|\boldsymbol{u}_o\| \geq 0$. These can model agents of higher priority, adversarial agents that are noncooperative to the motion of the class-A agents, or failed class-A agents whose motion is uncontrollable. In what follows, we refer to this class of dynamic obstacles as class-B agents [30]. We need the following assumptions to guarantee safety of the system in the presence these dynamic obstacles.

Assumption 4: The class-B agents are assumed to have circular shape with same size. The velocity of the class-B agents are bounded as $\|\boldsymbol{u}_o\| \leq u_o$ with $0 \leq u_o < \infty$.

Assumption 5: For any two class-B agents o_1, o_2 the interagent distance between the agents is $\|\boldsymbol{r}_{o_1}(t) - \boldsymbol{r}_{o_2}(t)\| > 2d_s$ for almost all $t \geq 0$ (i.e., any two class-B agents are not very close to each other at all times). Furthermore, for all class-B agents o, and for all $i \in \{1, \ldots, N\}$, $\|\boldsymbol{r}_o(t) - \boldsymbol{r}_{\text{gi}}\| \geq R_c + \delta_e$ for almost all $t \geq 0$ (i.e., the dynamic obstacles do not remain very close to the goal locations of the class-A agents at all times).

Remark 5: Assumption 5 is needed to guarantee that no class-A agent can become permanently occluded by a group of class-B agents and that they are not in conflict with class-B agents at their goal locations. Note that this is a sufficient condition to eliminate this situation. It might happen that, even if the class-B agents are very close to each other, the class-A agents are able to skip through and reach their goal location (see Sec. V for details).

Note that, unlike [30], we do not consider any communication between agents. The class-A agents do not even need to know whether their neighboring agents are of class-A or class-B. We are now ready to propose the coordination protocol for the multi-agent system in the presence of dynamic obstacles.

A. Safe Velocity Design

The desired linear velocity $\hat{\boldsymbol{u}}_{\text{id}}$ of each agent i is defined as per Eq. (22), where the modified $\hat{u}_{\text{id}}$ is given as

$$\hat{u}_{\text{id}} = \begin{cases} -\dfrac{1}{\mu}\log\left(\displaystyle\sum_{j\in\mathcal{N}_i|\hat{d}_{ij}\leq d_s} e^{-\mu\hat{u}^1_{\text{is}|j}}\right) & \hat{d}_{ij} \leq d_s, \\ -\dfrac{1}{\mu}\log\left(\displaystyle\sum_{j\in\mathcal{N}_i} e^{-\mu\hat{u}^1_{i|j}}\right), & d_s \leq d_{ij} \leq R_c, \\ u_{\text{ic}}, & d_{ij} > R_c; \end{cases} \tag{39}$$

where $\hat{u}^1_{i|j}$ is given by

$$\hat{u}^1_{i|j} = \hat{u}_{\text{ic}}\frac{\hat{d}_{ij} - d_s}{R_c - d_s} + \hat{u}^1_{\text{is}|j}\frac{R_c - \hat{d}_{ij}}{R_c - d_s} \tag{40}$$

where $\hat{u}^1_{\text{is}|j}$ is given as

$$\hat{u}^1_{\text{is}|j} = \begin{cases} (1+\varepsilon_i)\dfrac{\hat{\boldsymbol{r}}^T_{ji}\boldsymbol{u}^i_{\text{js}}}{\hat{\boldsymbol{r}}^T_{ji}\hat{\boldsymbol{u}}_{\text{id}n}}, & J_j > 0, \\ \varepsilon_i\dfrac{\hat{\boldsymbol{r}}^T_{ji}\boldsymbol{u}^i_{\text{js}}}{\hat{\boldsymbol{r}}^T_{ji}\hat{\boldsymbol{u}}_{\text{id}n}}, & J_j \leq 0; \end{cases} \tag{41}$$

where $\hat{J}_j = \hat{\boldsymbol{r}}^T_{ji}\hat{\boldsymbol{u}}^i_{\text{js}}$, and rest of the terms such as ε_i, $\hat{d}_{ij}$ are given as in Eq. (26).

Remark 6: Note that the expression in Eq. (39) is different from Eq. (24) because, in the latter case, we restrict the desired $\hat{u}_{\text{id}}$ to be always positive. In Eq. (39), we remove the $(+1)$ term in the argument of the logarithm, allowing $\hat{u}_{\text{id}}$ to take negative values as well.

B. Safety Analysis in the Presence of Dynamic Obstacles

With this definition of the desired velocity $\hat{\boldsymbol{u}}_{\text{id}}$ with $\hat{u}_{\text{id}}$ given by Eq. (39), we can state the following result.

Theorem 7: Consider N class-A agents $i \in \{1, \ldots, N\}$, assigned to move to goal locations $\boldsymbol{r}_{\text{gi}}$, and M class-B agents $o \in \{N+1, \ldots, N+M\}$, serving as dynamic obstacles satisfying Assumptions 4 and 5. Then, with d_s given as per Theorem 5, under the coordination protocol [Eq. (27)] with desired velocity defined as in Eq. (22) and $\hat{u}_{\text{id}}$ given as per Eq. (39), each class-A agent maintains safe distance d_m with other agents.

Proof: As per the analysis in Theorem 5, we obtain that, for any $j \in \mathcal{N}_i$, $\hat{d}_{ij} = \|\hat{\boldsymbol{r}}_i - \hat{\boldsymbol{r}}_j\| \geq d_s \Rightarrow \|\boldsymbol{r}_i - \boldsymbol{r}_j\| \geq d_m$. Thus, it is sufficient to prove that $\hat{d}_{ij} \geq d_s$ for all time t and for all $i \neq j$, i in class A, or equivalently, to prove that at $\hat{d}_{ij} = d_s$, the time derivative $\dot{\hat{d}}_{ij} \geq 0$. According to control law (39), the agent i adjusts its linear velocity u_i so that it avoids collision with the neighbor $j \in \mathcal{N}_i$ whose motion maximizes the rate of change of relative distance d_{ij}. Consider that $\hat{J}_j = \hat{\boldsymbol{r}}_{ji}^T \hat{\boldsymbol{u}}_{\text{js}}^i > 0$ (i.e., the class-B agent o is moving toward agent i). The time derivative of the interagent distance, evaluated at $\hat{d}_{ij} = d_s$, given by Eq. (29) under the closed-loop protocol [Eq. (39)], reads

$$\dot{\hat{d}}_{ij} = \frac{\hat{u}_{\text{id}} \hat{\boldsymbol{r}}_{ji}^T \hat{\boldsymbol{u}}_{\text{id}n} - \hat{\boldsymbol{r}}_{ji}^T \hat{\boldsymbol{u}}_{\text{js}}^i}{\hat{d}_{ij}} = \frac{(1+\varepsilon_i)\hat{\boldsymbol{r}}_{ji}^T \boldsymbol{u}_{\text{js}}^i - \hat{\boldsymbol{r}}_{ji}^T \hat{\boldsymbol{u}}_{\text{js}}^i}{\hat{d}_{ij}} = \frac{\varepsilon_i \hat{\boldsymbol{r}}_{ji}^T \boldsymbol{u}_{\text{os}}^i}{\hat{d}_{ij}} \geq 0$$

Similarly, when $\hat{J}_j = \hat{\boldsymbol{r}}_{ji}^T \hat{\boldsymbol{u}}_{\text{js}}^i \leq 0$ (i.e., agent j is moving away from agent i), the time derivative of the interagent distance at $\hat{d}_{ij} = d_s$ reads

$$\dot{\hat{d}}_{ij} = \frac{\hat{u}_{\text{id}} \hat{\boldsymbol{r}}_{ji}^T \hat{\boldsymbol{u}}_{\text{id}n} - \hat{\boldsymbol{r}}_{ji}^T \hat{\boldsymbol{u}}_{\text{js}}^i}{\hat{d}_{ij}} = \frac{\varepsilon_i \hat{\boldsymbol{r}}_{ji}^T \boldsymbol{u}_{\text{js}} - \hat{\boldsymbol{r}}_{ji}^T \hat{\boldsymbol{u}}_{\text{js}}^i}{\hat{d}_{ij}} = \frac{(\varepsilon_i - 1)\hat{\boldsymbol{r}}_{ji}^T \boldsymbol{u}_{\text{js}}^i}{\hat{d}_{ij}} \geq 0$$

Note that the last inequality is true because $0 < \varepsilon_i < 1$. Hence, every agent i maintains safe distance from its class-B neighbors. This shows that, in all possible scenarios, the class-A agent would maintain safe distance from all the other agents. □

C. Convergence Analysis

Theorem 8: Under the effect of coordination protocol (27) with desired velocity $\hat{\boldsymbol{u}}_{\text{id}}$ defined as in Eq. (22) and $\hat{u}_{\text{id}}$ given as per Eq. (39), the closed-loop trajectories [Eq. (1)] of each class-A agent i reach a δ_{ie} neighborhood around the goal location $\boldsymbol{r}_{\text{gi}}$ in finite time (i.e., $\exists T_i < \infty$), such that $\|\boldsymbol{r}_i(t) - \boldsymbol{r}_{\text{gi}}\| \leq \delta_{\text{ie}}(t)$ for all time $t \geq T_i$.

Proof: According to Assumption 5, there are no two class-B agents whose distance is less than $2d_s$ for all times, which implies that there would always be space between the two obstacles from where the class-A agent can skip through. The rest of the proof directly follows from Theorem 6. Also, because the class-B agents are not always near the goal locations $\boldsymbol{r}_{\text{gi}}$ (Assumption 5), once the class-A agent i reaches its goal location, it can stay there.

Remark 7: Although as per Lemma 1, there would be no deadlocks in the motion of the agents, it is still possible that there are livelocks. Livelock occurs when periodic motions are executed by the agents, which can be induced either by periodic motion of class-B agents or by carefully choosing the control gains, the direction of the wind, and the set of initial and goal locations for the class-A agents. Excluding the livelocks is a rather difficult problem, is out of scope of the current work, and is left as a problem for future investigation.

Hence, we showed that, in the presence of moving obstacles or class-B agents, the class-A agents would be able to reach very close to the desired goal location while maintaining safety. Next, we present a few simulation results to show the efficacy of the proposed control design.

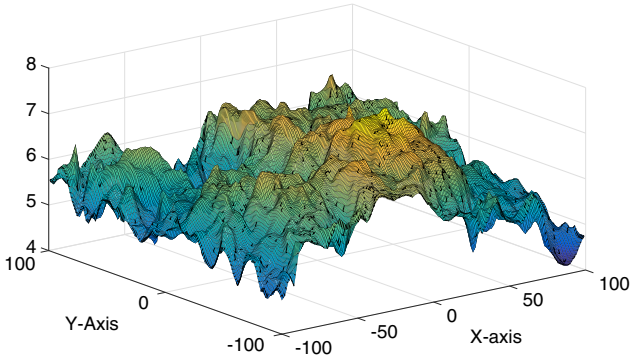

Fig. 3 Wind profile used as external disturbance.

V. Simulations

We consider five scenarios. The first three scenarios involve $N = 46$ agents, out of which 20 are class-B agents, and 26 are class-A agents; the fourth scenario involves three class-A and three class-B agents; and the fifth scenario includes $N = 48$ class-A agents, which are assigned to move toward goal locations while avoiding collisions. The goal locations are selected sufficiently far apart so that the agents' sensing regions do not overlap when agents lie on their goal locations (i.e., $\|\boldsymbol{r}_{\text{gi}} - \boldsymbol{r}_{\text{gj}}\| > R_c$ for $i \neq j$). The simulation parameters for all the four scenarios are listed next.

1) $d_m = 4$ m, $\epsilon_s = 5$, $\delta_e = 15$, $d_s = 29$ m, and $R_c = 3.5d_s$. Define $\Delta_e = \max_i\{l_i \delta_w^{c_i}\}$, so that, from Theorem 8, we have $\|\boldsymbol{r}_{\text{ie}}\| \leq \Delta_e$ for all times $t \geq \max_i T_i$. In our case, $\Delta_e = 0.8824$ m.

2) $\boldsymbol{w}_{\text{av}} = [5.86, 2.96]^T$ m/s and $\delta_w = 1.92$ m/s.

3) $\varepsilon_i = 0.01$, $k_{i1} = 5$, $k_{i3} = 0.8538$, $k_{i4} = 0.3149$, $\alpha_r = 0.9$, $R_1 = 0.4017$ m, $\alpha_1 = 0.9$, and $\alpha_2 = 0.8$.

Figure 3 shows the spatial variation of the wind speed used as the external disturbance in the simulations. The magnitude of the wind (i.e., the wind speed) at each x–y location is plotted. The figure shows the variation of the wind speed in the x–y plane in the domain $[-100, 100] \times [-100, 100]$. In simulations, we used the following formulation to scale up the domain of the disturbance:

$$\boldsymbol{w}(x \pm 200, y \pm 200, t) = \boldsymbol{w}(x, y, t) \tag{42}$$

We choose the goal locations such that they form the characters UM for the aesthetic appeal of the simulations. In Fig. 4, the initial positions of the agents are marked by diamonds; blue diamonds are the initial positions of class-A agents, and red diamonds are those of class-B agents. In the first scenario, class-B agents are moving outward, whereas class-A agents are coming inward. The black ellipse is used to denote the agents that are moving in the same direction with arrows representing their direction of motion. In scenario 2, the class-B agents (red diamonds) start in V-formation as represented by the black lines.

We present five simulation scenarios. The simulation videos for all five scenarios can be found at online.[§] In the first two scenarios, the class-B agents are such that the Assumption 5 is satisfied, whereas in scenario 3, the motion of class-B agents is chosen such that Assumption 5 is not satisfied.

1) In the first scenario, the class-B agents start in between the class-A agents and move outward, whereas class-A agents move inward. The set of initial locations, target locations, and initial directions of movement are given in Fig. 4. This scenario shows how effectively class-A agents can avoid collisions with class-B agents. Furthermore, we assume that the wind disturbance in this case varies only with $\boldsymbol{r}$ and is constant in t, i.e., $\boldsymbol{w} = \boldsymbol{w}(\boldsymbol{r})$ (see Figs. 5 and 6).

2) In the second scenario, the class-B agents come as a swarm in the V-formation toward the class-A agents. This scenario shows how class-A agents can avoid collisions with other class-A agents

[§]Data available online at https://www.dropbox.com/s/hu2beebxybqo20y/AIAA_JGCD_Sim.avi?dl=0 [retrieved 17 February 2019].

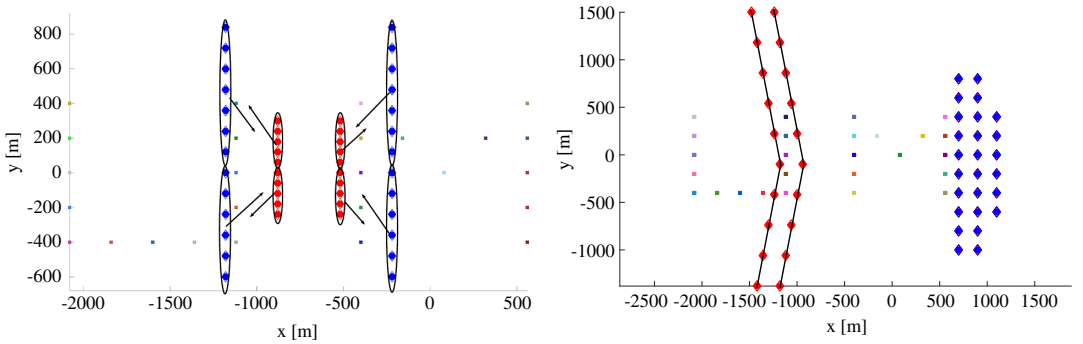

Fig. 4 Initial configuration of scenarios 1 and 2.

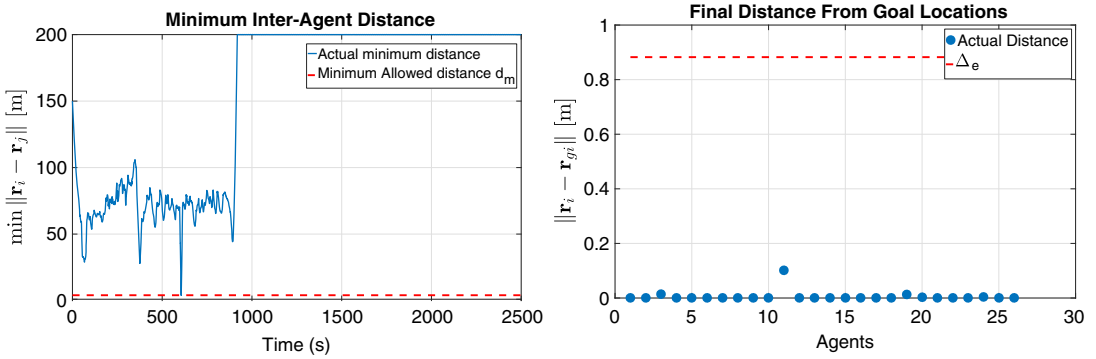

Fig. 5 Scenario 1: (safety) minimum interagent distance and (convergence) final distance from the goal.

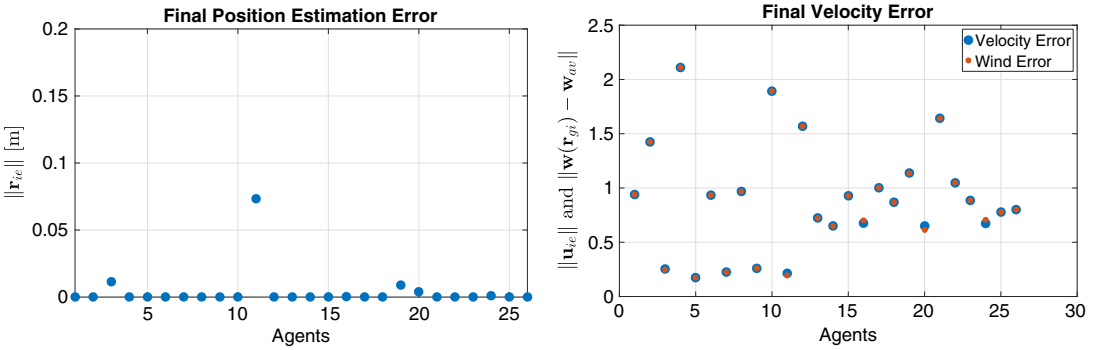

Fig. 6 Scenario 1: final position error $\|r_{ie}\|$, velocity estimation error $\|u_{ie}\|$, and $\|w(r_{gi},t) - w_{av}\|$.

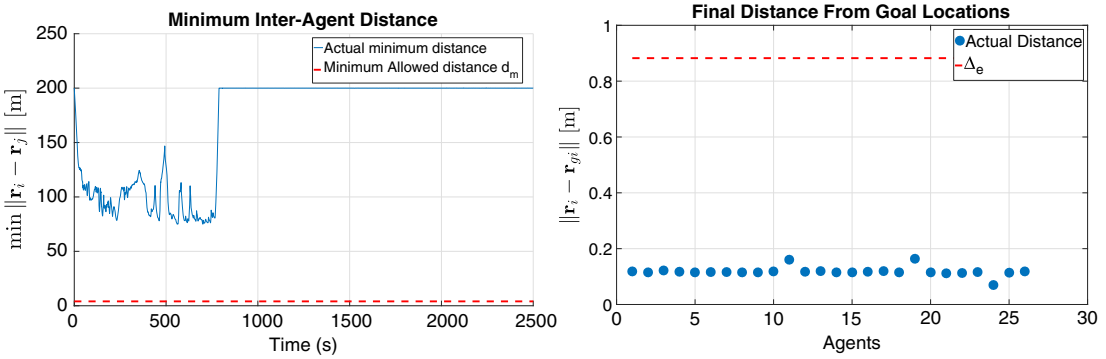

Fig. 7 Scenario 2: (safety) minimum interagent distance and (convergence) final distance from the goal.

and class-B agents all together. In this case, we allow the wind disturbance to vary in both space and time, i.e., $\boldsymbol{w} = \boldsymbol{w}(\boldsymbol{r}, t)$. We discuss the difference in the results in the first two scenarios arising because of the difference in assumptions on the wind disturbance (see Figs. 7–9).

3) In the third scenario, Assumption 5 is allowed to be violated (i.e., the class-B agents move very closely to each other). In this case, as can be seen in Fig. 10, we observe that the class-A agents become occluded by the formation of class-B agents and do not reach their desired locations. But after some time, it is observed that some of the

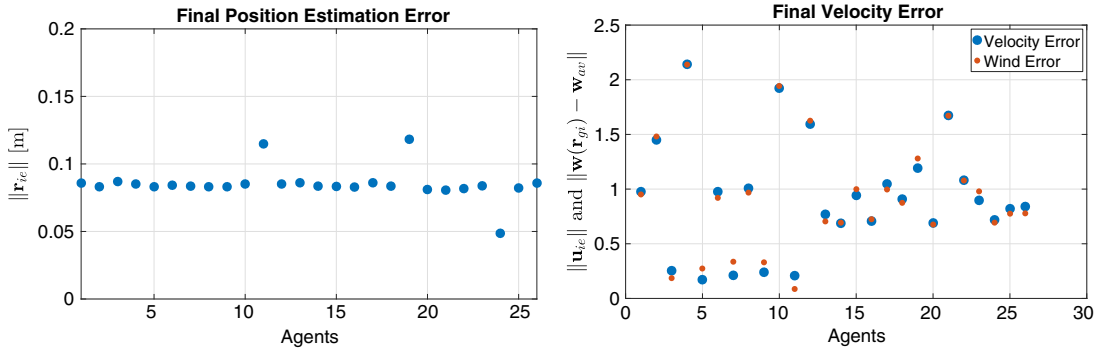

Fig. 8 Scenario 2: final position error $\|r_{ie}\|$, velocity estimation error $\|u_{ie}\|$, and error term $\|w(r_{gi},t) - w_{av}\|$.

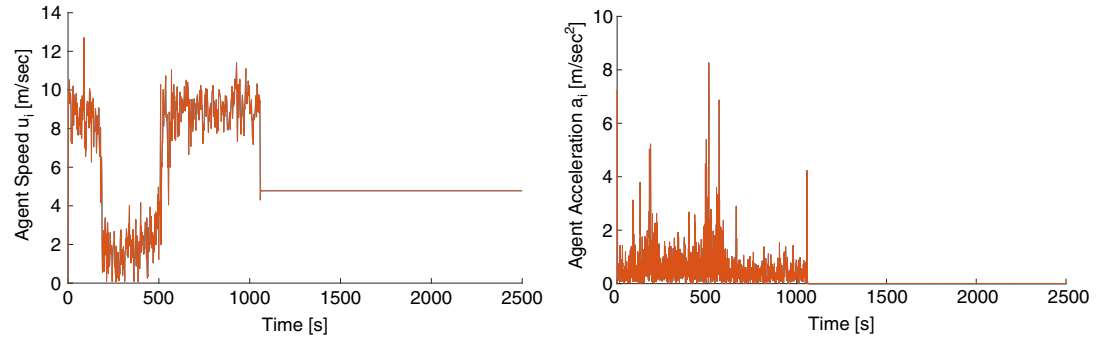

Fig. 9 Magnitude of velocity and acceleration of a class-A agent.

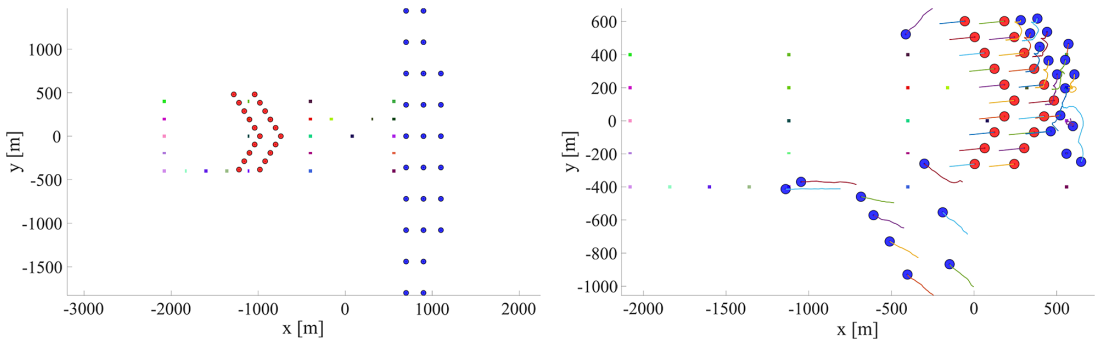

Fig. 10 Scenario 3: violation of Assumption 5. Dynamic obstacles come in a V-formation. Snapshots at $T = 0$ and $T = 280$ s. The trails show the paths of the agents for last 60 s.

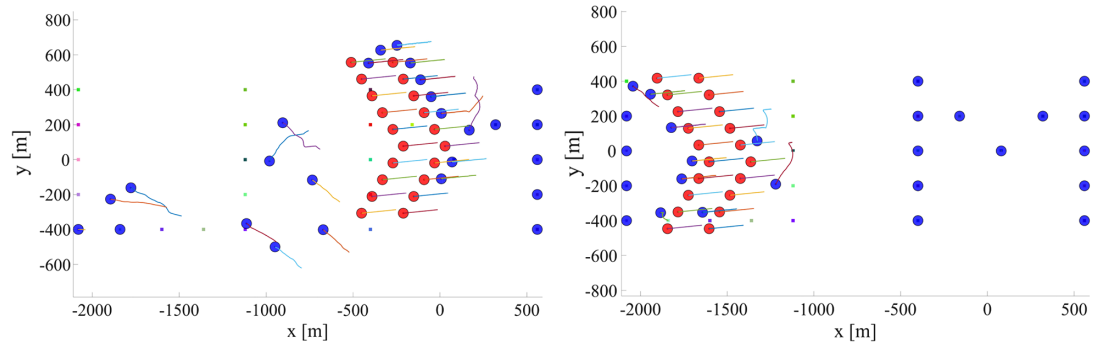

Fig. 11 Scenario 3: herding of class-A agents. The class-A agents have become occluded and herded by the formation of class-B agents. Snapshots at $T = 420$ and $T = 700$ s.

class-A agents manage to escape through; see Figs. 10–12 and Sec. VI. In the fourth scenario, with three class-A and three class-B agents, we allow Assumption 5 to be violated; see Fig. 13.

4) In the fifth scenario, we consider 48 class-A agents with initial and goal locations chosen on two concentric circles. Figure 14 shows the initial configuration of the agents and their desired goal locations, whereas Figs. 15 and 16 show the simulation snapshots at various time instants.

In Figs. 4, 10–16, class-A agents are colored blue, whereas class-B agents are colored red. Figures 5, 7, and 17 show the performance of the presented protocol both in terms of safety and convergence. In all the figures, it can be seen that class-A agents are able to maintain safe

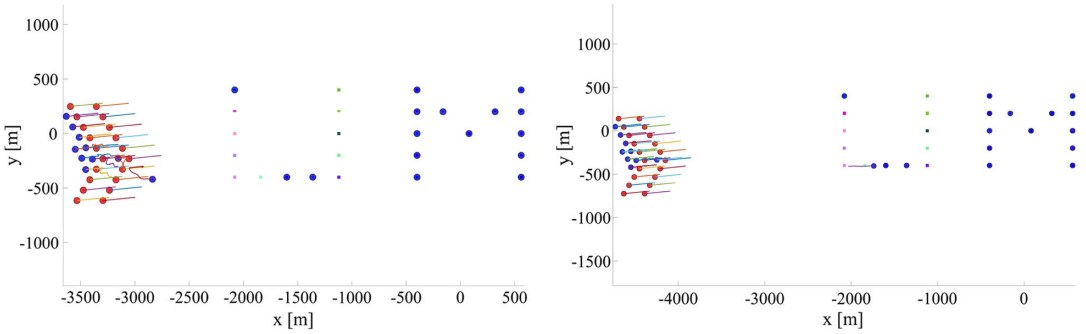

Fig. 12 Scenario 3: after some time, one of the class-A agents is able to escape the occlusion caused by the motion of class-B agents. Snapshots at $T = 1120$ and $T = 1260$ s.

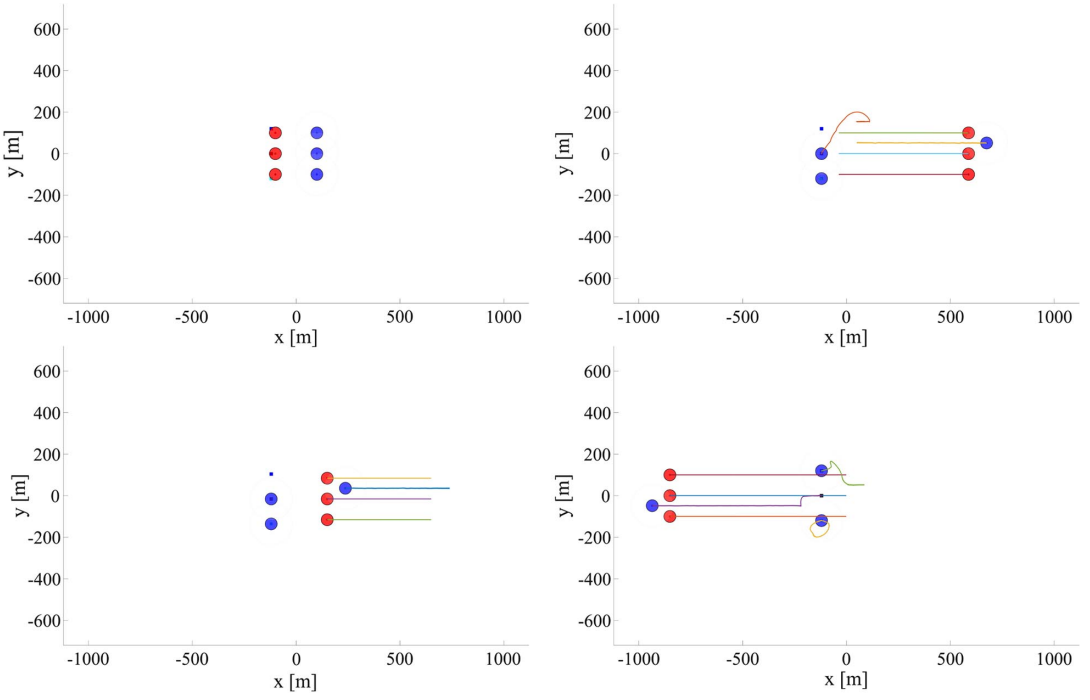

Fig. 13 Three-agent scenario: herding of class-A agents. Snapshots at $T = 0, 200, 400, 600$ s. Trails show the paths traced by agents in the last 150 s.

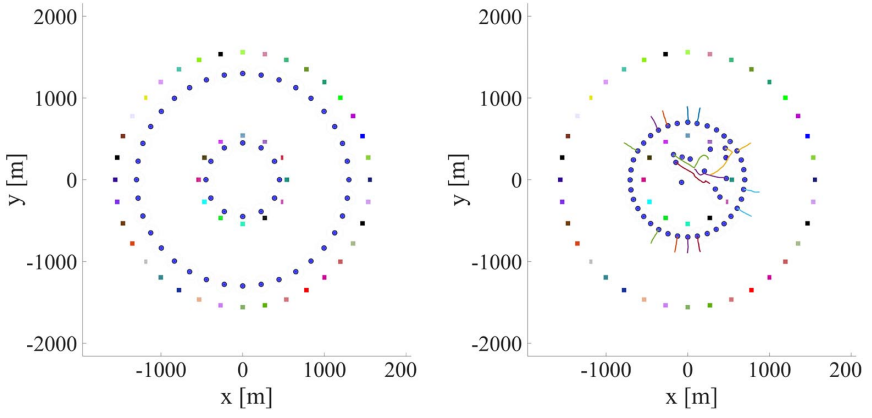

Fig. 14 Scenario 5: initial and goal locations of the 48 agents. Snapshots at $T = 0$ and $T = 120$ s.

distance d_m with all the other agents (both class-A and class-B agents). Also, it can be seen that the class-A agents reach a much smaller neighborhood of their desired goal locations (i.e., their final distance from their goal location $\|\boldsymbol{r}_i - \boldsymbol{r}_{\text{gi}}\|$) than the theoretical (conservative) bound given as per Theorem 8.

Note that, for the observer dynamics [Eq. (19)], the equilibrium point is $\boldsymbol{r}^*_{\text{ie}}(t) = 0$, and $\boldsymbol{u}^*_{\text{ie}}(t) = -(\boldsymbol{w}(\boldsymbol{r}_i, t) - \boldsymbol{w}_{\text{av}})$. Because this equilibrium point varies in both space and time, and we do not assume anything about the time derivative of the disturbance $\boldsymbol{w}(\boldsymbol{r}_i, t)$, we cannot prove that system (19) would actually stay at this time-varying equilibrium. As can be seen in Fig. 6, the error $\|\boldsymbol{r}_{\text{ie}}\|$ is close to 0, whereas $\|\boldsymbol{u}_{\text{ie}}(t)\|$ is close to $\|\boldsymbol{w}(\boldsymbol{r}_{\text{gi}}, t) - \boldsymbol{w}_{\text{av}}\|$ under the assumption that $\boldsymbol{w}(\boldsymbol{r}_i, t)$ does not vary with time. In the case when the wind is indeed a function of time, we can see from Fig. 8 that, although the

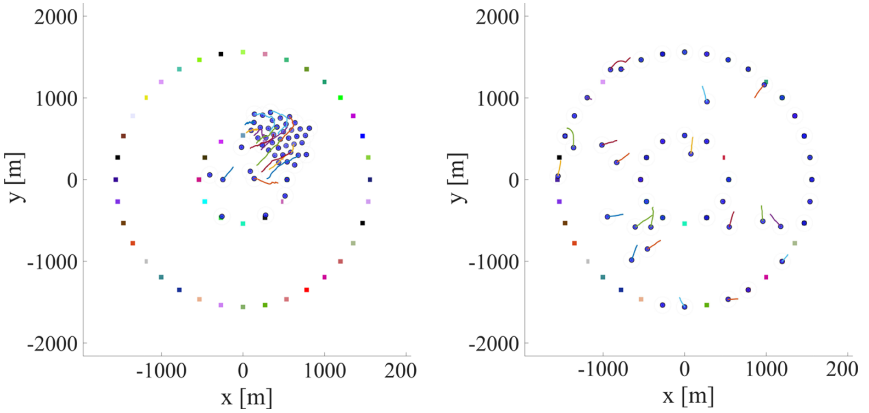

Fig. 15 Scenario 5: all class-A agents come very close to each other. Snapshots at $T = 240$ and $T = 480$ s.

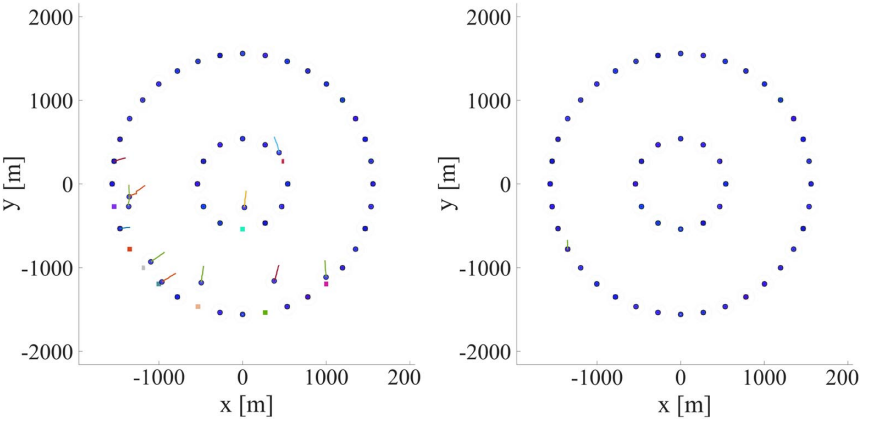

Fig. 16 Scenario 5: agents are able to resolve conflicts and reach their goal locations. Snapshots at $T = 600$ and $T = 720$ s.

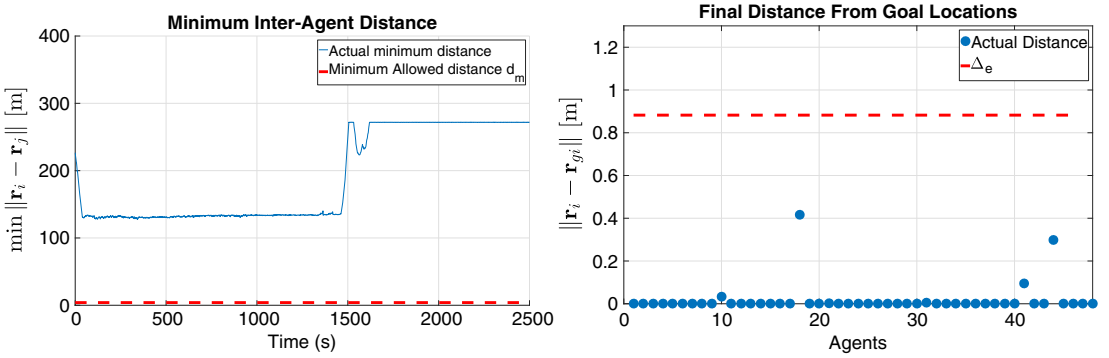

Fig. 17 Scenario 4: (safety) minimum interagent distance and (convergence) final distance from the goal.

final estimation error is still very small, the velocity error does not converge to the actual wind error.

Figure 9 shows the norm of the accelerations and the velocities of one of the class-A agents. Once the class-A agent reaches its goal location, its velocity becomes constant, equal and opposite of the wind disturbance at the location, and the acceleration becomes zero. The commanded acceleration and the velocity are noisy because of the disturbance $\boldsymbol{w}$ and the sensing uncertainties.

In Figs. 10–12 and 14–16, the trails show the path traced by the agents in the last 60 s. The class-A agents are colored blue, whereas the class-B agents are colored red. Figures 10 and 11 show the snapshots of the simulation when a few of the class-A agents get trapped in between the formation of class-B agents. Figure 12 shows how one of the class-A agents manages to escape from the formation and moves toward its goal location. This shows that, even if Assumption 5 is violated, the class-A agents can still resolve the conflicts with class-B agents and reach their goal locations. To see the resulting motion of the class-A agents, the reader is requested to see the video at the link provided in the beginning of Sec. V. For the sake of demonstration, we present a smaller simulation scenario with three class-A and three class-B agents in Fig. 13 for the case when Assumption 5 is violated. The traces show the paths of the agents for last 150 s. We can see that the class-B agents are able to trap the class-A agents.

In the last scenario, we simulated 48 class-A agents and chose the initial and final locations symmetrically around concentric circles, such that all the agents meet in the center. Figure 14 shows the initial and the goal locations and the snapshots at different time instants of the agents in scenario 5. Figures 15 and 16 show the snapshots of the simulation of scenario 5 at various time instants, whereas Fig. 17 shows the minimum interagent distance and their final distances from their respective goal locations. It is clear that the agents are able to resolve all the conflicts and reach their goal locations in finite time.

VI. Discussions

As demonstrated via various simulation scenarios, our proposed protocol can deconflict a large number of agents while maintaining safety and guaranteed convergence to the neighborhood of the desired goal location in the presence of unknown state disturbances. The main strength of the proposed approach is the scalability with the number of agents and the ability to counteract a class of state disturbance and sensing uncertainties. One of the main drawbacks of the presented work is the assumption on the motion of the dynamic obstacles. It is important to note that Assumption 5 is a sufficient condition to avoid the herding of the class-A agents by a formation of class-B agents. Furthermore, it is needed that the class-B agents do not hover around the goal location of the class-A agents, so that there is no conflict once the class-A agents reach their respective goal locations. As demonstrated in scenario 3 in the simulations, even if this condition fails to hold, the class-A agents can still reach their goal locations. This is due to the fact that the external disturbance $\boldsymbol{w}$ and the sensing uncertainty in the positions of the neighboring agents can result in a vector field taking the class-A agents through the narrow gap between the class-B agents while maintaining safety.

In this work, we assumed that the velocity of the dynamic obstacle is upper-bounded but did not use it in the control design. One of the directions of the future work is identification of the noncooperative neighbors. Once a class-A agent identifies a dynamic obstacle, it can use the knowledge of the upper bound on the velocity of the obstacle to avoid the herding.

VII. Conclusions

A robust distributed estimation and control scheme to generate collision-free trajectories for multiple agents in the presence of dynamic obstacles and unmatched state disturbances standing for wind effects were presented. It was proved that, under the adopted disturbance (dynamic obstacle and wind) modeling and assumptions, the safety and convergence of the system can be guaranteed. A finite-time observer and a finite-time feedback controller were designed, and it was proved that the closed trajectories of each agent converge to a δ neighborhood of their respective goal locations in a finite time, where δ depends upon the external disturbances acting on the system. The proposed method, being completely distributed with analytical expressions for the observer and control laws, is scalable with the number of agents.

Acknowledgments

The authors would like to acknowledge the support of NASA (grant NNX16AH81A) and the U.S. Air Force Office of Scientific Research (award number FA9550-17-1-0284). The authors would also like to thank the associate editor and the anonymous reviewers for their valuable comments and suggestions to improve the quality of the paper.

References

[1] Klausen, K., Fossen, T. I., Johansen, T. A., and Aguiar, A. P., "Cooperative Path-Following for Multirotor UAVs with a Suspended Payload," *2015 IEEE Conference on Control Applications*, IEEE Publ., Piscataway, NJ, 2015, pp. 1354–1360. doi:10.1109/CCA.2015.7320800

[2] Quintero, S. A., Collins, G. E., and Hespanha, J. P., "Flocking with Fixed-Wing UAVs for Distributed Sensing: A Stochastic Optimal Control Approach," *2013 American Control Conference*, IEEE Publ., Piscataway, NJ, 2013, pp. 2025–2031. doi:10.1109/ACC.2013.6580133

[3] Ren, W., and Cao, Y., "Overview of Recent Research in Distributed Multi-Agent Coordination," *Distributed Coordination of Multi-Agent Networks*, Communications and Control Engineering, Springer–Verlag, London, England, 2011, pp. 23–41, Chap. 2. doi:10.1109/TII.2012.2219061

[4] Knorn, S., Chen, Z., and Middleton, R. H., "Overview: Collective Control of Multiagent Systems," *IEEE Transactions on Control of Network Systems*, Vol. 3, No. 4, 2016, pp. 334–347. doi:10.1109/TCNS.2015.2468991

[5] Peterson, C., and Paley, D. A., "Multivehicle Coordination in an Estimated Time-Varying Flowfield," *Journal of Guidance, Control, and Dynamics*, Vol. 34, No. 1, 2011, pp. 177–191. doi:10.2514/1.50036

[6] Lee, J.-W., Walker, B., and Cohen, K., "Path Planning of Unmanned Aerial Vehicles in a Dynamic Environment," *Infotech@Aerospace 2011*, AIAA Paper 2011-1654, 2011. doi:10.2514/6.2011-1654

[7] Alonso-Mora, J., Naegeli, T., Siegwart, R., and Beardsley, P., "Collision Avoidance for Aerial Vehicles in Multi-Agent Scenarios," *Autonomous Robots*, Vol. 39, No. 1, 2015, pp. 101–121. doi:10.1007/s10514-015-9429-0

[8] Chen, Y., Cutler, M., and How, J. P., "Decoupled Multiagent Path Planning via Incremental Sequential Convex Programming," *2015 IEEE International Conference on Robotics and Automation*, IEEE Publ., Piscataway, NJ, 2015, pp. 5954–5961. doi:10.1109/ICRA.2015.7140034

[9] Panagou, D., Stipanović, D. M., and Voulgaris, P. G., "Distributed Coordination Control for Multi-Robot Networks Using Lyapunov-Like Barrier Functions," *IEEE Transactions on Automatic Control*, Vol. 61, No. 3, 2016, pp. 617–632. doi:10.1109/TAC.2015.2444131

[10] Glotfelter, P., Cortés, J., and Egerstedt, M., "Nonsmooth Barrier Functions with Applications to Multi-Robot Systems," *IEEE Control Systems Letters*, Vol. 1, No. 2, 2017, pp. 310–315. doi:10.1109/LCSYS.2017.2710943

[11] Choi, J.-W., Curry, R., and Elkaim, G., "Real-Time Obstacle-Avoiding Path Planning for Mobile Robots," *AIAA Guidance, Navigation, and Control Conference*, AIAA Paper 2010-8411, 2010. doi:10.2514/6.2010-8411

[12] Wilburm, J., Perhinschi, M., Wilburn, B., and Karas, O., "Development of a Modified Voronoi Algorithm for UAV Path Planning and Obstacle Avoidance," *AIAA Guidance, Navigation, and Control Conference*, AIAA Paper 2012-4904, 2012. doi:10.2514/6.2012-4904

[13] Chen, T., Zhang, G., Hu, X., and Xiao, J., "Unmanned Aerial Vehicle Route Planning Method Based on a Star Algorithm," *2018 13th IEEE Conference on Industrial Electronics and Applications*, IEEE Publ., Piscataway, NJ, 2018, pp. 1510–1514. doi:10.1109/ICIEA.2018.8397948

[14] Chen, G., Shen, D., Cruz, J., Kwan, C., Riddle, S., Cox, S., and Matthews, C., "A Novel Cooperative Path Planning for Multiple Aerial Platforms," *Infotech@Aerospace*, AIAA Paper 2005-6948, 2005. doi:10.2514/6.2005-6948

[15] Aoude, G. S., Luders, B. D., Joseph, J. M., Roy, N., and How, J. P., "Probabilistically Safe Motion Planning to Avoid Dynamic Obstacles with Uncertain Motion Patterns," *Autonomous Robots*, Vol. 35, No. 1, 2013, pp. 51–76. doi:10.1007/s10514-013-9334-3

[16] Frazzoli, E., Dahleh, M. A., and Feron, E., "Real-Time Motion Planning for Agile Autonomous Vehicles," *Journal of Guidance, Control, and Dynamics*, Vol. 25, No. 1, 2002, pp. 116–129. doi:10.2514/2.4856

[17] Elbanhawi, M., and Simic, M., "Sampling-Based Robot Motion Planning: A Review," *IEEE Access*, Vol. 2, Jan. 2014, pp. 56–77. doi:10.1109/ACCESS.2014.2302442

[18] LaValle, S. M., *Planning Algorithms*, Cambridge Univ. Press, Cambridge, England, 2006, Chaps. 2, 6. doi:10.1017/CBO9780511546877

[19] Choset, H., Lynch, K., Hutchinson, S., Kantor, G., Burgard, W., Kavraki, L., and Thrun, S., *Principles of Robot Motion. Theory, Algorithms and Implementation*, MIT Press, Cambridge, MA, 2005, Chaps. 4, 7. doi:10.1017/S0263574706212803

[20] Leitmann, G., and Skowronski, J., "Avoidance Control," *Journal of Optimization Theory and Applications*, Vol. 23, Dec. 1977, pp. 581–591. doi:10.1007/BF00933298

[21] Hernandez-Martinez, E. G., and Aranda-Bricaire, E., "Convergence and Collision Avoidance in Formation Control: A Survey of the Artificial Potential Functions Approach," *Multi-Agent Systems: Modeling, Control, Programming, Simulations and Applications*, edited by F. Alkhateeb, E. A. Maghayreh, and I. A. Doush, InTech, London, England, 2011, pp. 103–126. doi:10.5772/14142

[22] Dimarogonas, D. V., and Kyriakopoulos, K. J., "Connectedness Preserving Distributed Swarm Aggregation for Multiple Kinematic Robots," *IEEE Transactions on Robotics*, Vol. 24, No. 5, 2008,

pp. 1213–1223.
doi:10.1109/TRO.2008.2002313
[23] Cheng, T.-H., Kan, Z., Rosenfeld, J. A., and Dixon, W. E., "Decentralized Formation Control with Connectivity Maintenance and Collision Avoidance Under Limited and Intermittent Sensing," *2014 American Control Conference*, IEEE Publ., Piscataway, NJ, 2014, pp. 3201–3206.
doi:10.1109/ACC.2014.6859177
[24] Szulczyński, P., Pazderski, D., and Kozłowski, K., "Real-Time Obstacle Avoidance Using Harmonic Potential Functions," *Journal of Automation, Mobile Robotics and Intelligent Systems*, Vol. 5, No. 3, 2011, pp. 59–66.
[25] Liddy, T., Lu, T.-F., Lozo, P., and Harvey, D., "Obstacle Avoidance Using Complex Vector Fields," *Proceedings of the 2008 Australasian Conference on Robotics and Automation*, Australian Robotics and Automation Association, Canberra, Australia, 2008.
[26] Hernández-Martínez, E. G., and Aranda-Bricaire, E., "Multi-Agent Formation Control with Collision Avoidance Based on Discontinuous Vector Fields," *Proceedings of the 35th Annual Conference of IEEE Industrial Electronics*, IEEE Publ., Piscataway, NJ, 2009, pp. 2283–2288.
doi:10.1109/IECON.2009.5415217
[27] Flores-Resendiz, J., Aranda-Bricaire, E., González-Sierra, J., and Santiaguillo-Salinas, J., "Finite-Time Formation Control Without Collisions for Multiagent Systems with Communication Graphs Composed of Cyclic Paths," *Mathematical Problems in Engineering*, Vol. 2015, Jan. 2015, Paper 948086.
doi:10.1155/2015/948086
[28] Rodrguez-Seda, E. J., Tang, C., Spong, M. W., and Stipanović, D. M., "Trajectory Tracking with Collision Avoidance for Nonholonomic Vehicles with Acceleration Constraints and Limited Sensing," *International Journal of Robotics Research*, Vol. 33, No. 12, 2014, pp. 1569–1592.
doi:10.1177/0278364914537130
[29] Rodrguez-Seda, E. J., Stipanović, D. M., and Spong, M. W., "Guaranteed Collision Avoidance for Autonomous Systems with Acceleration Constraints and Sensing Uncertainties," *Journal of Optimization Theory and Applications*, Vol. 168, No. 3, 2016, pp. 1014–1038.
doi:10.1007/s10957-015-0824-7
[30] Panagou, D., "A Distributed Feedback Motion Planning Protocol for Multiple Unicycle Agents of Different Classes," *IEEE Transactions on Automatic Control*, Vol. 62, No. 3, 2017, pp. 1178–1193.
doi:10.1109/TAC.2016.2576020
[31] Ahn, H., Colombo, A., and Del Vecchio, D., "Supervisory Control for Intersection Collision Avoidance in the Presence of Uncontrolled Vehicles," *2014 American Control Conference*, IEEE Publ., Piscataway, NJ, 2014, pp. 867–873.
doi:10.1109/ACC.2014.6859163
[32] Ahn, H., Rizzi, A., Colombo, A., and Del Vecchio, D., "Robust Supervisors for Intersection Collision Avoidance in the Presence of Uncontrolled Vehicles," *arXiv preprint arXiv:1603.03916*, March 2016, https://arxiv.org/abs/1603.03916.
[33] Trentelman, H. L., Takaba, K., and Monshizadeh, N., "Robust Synchronization of Uncertain Linear Multi-Agent Systems," *IEEE Transactions on Automatic Control*, Vol. 58, No. 6, 2013, pp. 1511–1523.
doi:10.1109/TAC.2013.2239011
[34] Liu, X., Ho, D. W., Cao, J., and Xu, W., "Discontinuous Observers Design for Finite-Time Consensus of Multiagent Systems with External Disturbances," *IEEE Transactions on Neural Networks and Learning Systems*, Vol. 28, No. 11, 2017, pp. 2826–2830.
doi:10.1109/TNNLS.2016.2599199
[35] Fu, J., and Wang, J., "Fixed-Time Coordinated Tracking for Second-Order Multi-Agent Systems with Bounded Input Uncertainties," *Systems & Control Letters*, Vol. 93, July 2016, pp. 1–12.
doi:10.1016/j.sysconle.2016.03.006
[36] Hong, H., Yu, W., Wen, G., and Yu, X., "Distributed Robust Fixed-Time Consensus for Nonlinear and Disturbed Multiagent Systems," *IEEE Transactions on Systems, Man, and Cybernetics: Systems*, Vol. 47, No. 7, 2017, pp. 1464–1473.
doi:10.1109/TSMC.2016.2623634
[37] Wang, X., and Li, S., "Distributed Finite-Time Consensus Algorithms for Leader–Follower Second-Order Multi-Agent Systems with Mismatched Disturbances," *American Control Conference*, IEEE Publ., Piscataway, NJ, 2016, pp. 2814–2819.
doi:10.1109/ACC.2016.7525345
[38] Li, P., Qin, K., and Shi, M., "Distributed Robust H Infinity Rotating Consensus Control for Directed Networks of Second-Order Agents with Mixed Uncertainties and Time-Delay," *Neurocomputing*, Vol. 148, Jan. 2015, pp. 332–339.
doi:10.1016/j.neucom.2014.06.063
[39] Rezaei, V., and Stefanovic, M., "Distributed Leaderless and Leader–Follower Consensus of Linear Multiagent Systems Under Persistent Disturbances," *2016 24th Mediterranean Conference on Control and Automation*, IEEE Publ., Piscataway, NJ, 2016, pp. 587–592.
doi:10.1109/MED.2016.7536062
[40] Wang, X., Saberi, A., Stoorvogel, A. A., and Grip, H. F., "Control of a Chain of Integrators Subject to Actuator Saturation and Disturbances," *International Journal of Robust and Nonlinear Control*, Vol. 22, No. 14, 2012, pp. 1562–1570.
doi:10.1002/rnc.1767
[41] Wang, X., Li, S., Yu, X., and Yang, J., "Distributed Active Anti-Disturbance Consensus for Leader–Follower Higher-Order Multi-Agent Systems with Mismatched Disturbances," *IEEE Transactions on Automatic Control*, Vol. 62, No. 11, 2017, pp. 5795–5801.
doi:10.1109/TAC.2016.2638966
[42] Tian, B., Lu, H., Zuo, Z., and Zong, Q., "Multivariable Uniform Finite-Time Output Feedback Reentry Attitude Control for RLV with Mismatched Disturbance," *Journal of the Franklin Institute*, Vol. 355, No. 8, 2018, pp. 3470–3487.
doi:10.1016/j.jfranklin.2018.01.042
[43] Garg, K., Han, D., and Panagou, D., "Robust Semi-Cooperative Multi-Agent Coordination in the Presence of Stochastic Disturbances," *2017 IEEE 56th Annual Conference on Decision and Control*, IEEE Publ., Piscataway, 2017, pp. 3443–3448.
doi:10.1109/CDC.2017.8264163
[44] Garg, K., and Panagou, D., "A Robust Coordination Protocol for Safe Multi-Agent Motion Planning," *2018 AIAA Guidance, Navigation, and Control Conference*, AIAA Paper 2018-0605, 2018.
doi:10.2514/6.2018-0605
[45] Ryan, E., "Finite-Time Stabilization of Uncertain Nonlinear Planar Systems," *Dynamics and Control*, Vol. 1, Springer, Dordrecht, The Netherlands, 1991, pp. 83–94.
doi:10.1007/BF02169426
[46] Bhat, S. P., and Bernstein, D. S., "Finite-Time Stability of Continuous Autonomous Systems," *SIAM Journal on Control and Optimization*, Vol. 38, No. 3, 2000, pp. 751–766.
doi:10.1137/S0363012997321358
[47] Bhat, S. P., and Bernstein, D. S., "Geometric Homogeneity with Applications to Finite-Time Stability," *Mathematics of Control, Signals and Systems*, Vol. 17, No. 2, 2005, pp. 101–127.
doi:10.1007/s00498-005-0151-x
[48] Wang, X., and Hong, Y., "Finite-Time Consensus for Multi-Agent Networks with Second-Order Agent Dynamics," *IFAC Proceedings Volumes*, Vol. 41, No. 2, 2008, pp. 15185–15190.
doi:10.3182/20080706-5-KR-1001.02568
[49] Xiao, F., Wang, L., Chen, J., and Gao, Y., "Finite-Time Formation Control for Multi-Agent Systems," *Automatica*, Vol. 45, No. 11, 2009, pp. 2605–2611.
doi:10.1016/j.automatica.2009.07.012
[50] Liu, Y., and Geng, Z., "Finite-Time Formation Control for Linear Multi-Agent Systems: A Motion Planning Approach," *Systems & Control Letters*, Vol. 85, Nov. 2015, pp. 54–60.
doi:10.1016/j.sysconle.2015.08.009
[51] Li, S., and Wang, X., "Finite-Time Consensus and Collision Avoidance Control Algorithms for Multiple AUVs," *Automatica*, Vol. 49, No. 11, 2013, pp. 3359–3367.
doi:10.1016/j.automatica.2013.08.003
[52] Li, S., Du, H., and Lin, X., "Finite-Time Consensus Algorithm for Multi-Agent Systems with Double-Integrator Dynamics," *Automatica*, Vol. 47, No. 8, 2011, pp. 1706–1712.
doi:10.1016/j.automatica.2011.02.045
[53] Hu, J., Li, S., Zhao, C., Pan, Q., Fan, B., Zhang, Z., and Li, H., "Finite-Time Consensus for Multi UAV System with Collision Avoidance," *2017 IEEE International Conference on Unmanned Systems*, IEEE Publ., Piscataway, NJ, 2017, pp. 517–522.
doi:10.1109/ICUS.2017.8278400
[54] Ma, J., and Lai, E. M., "Finite-Time Flocking Control of a Swarm of Cucker–Smale Agents with Collision Avoidance," *2017 24th International Conference on Mechatronics and Machine Vision in Practice*, IEEE Publ., Piscataway, NJ, 2017, pp. 1–6.
doi:10.1109/M2VIP.2017.8211507
[55] Wang, L., Sun, S., and Xia, C., "Finite-Time Stability of Multi-Agent System in Disturbed Environment," *Nonlinear Dynamics*, Vol. 67, No. 3, 2012, pp. 2009–2016.
doi:10.1007/s11071-011-0125-0

[56] Zuo, Z., and Tie, L., "Distributed Robust Finite-Time Nonlinear Consensus Protocols for Multi-Agent Systems," *International Journal of Systems Science*, Vol. 47, No. 6, 2016, pp. 1366–1375. doi:10.1080/00207721.2014.925608

[57] Defoort, M., Polyakov, A., Demesure, G., Djemai, M., and Veluvolu, K., "Leader–Follower Fixed-Time Consensus for Multi-Agent Systems with Unknown Non-Linear Inherent Dynamics," *IET Control Theory & Applications*, Vol. 9, No. 14, 2015, pp. 2165–2170. doi:10.1049/iet-cta.2014.1301

[58] Ma, X., Jiao, Z., Wang, Z., and Panagou, D., "3-D Decentralized Prioritized Motion Planning and Coordination for High-Density Operations of Micro Aerial Vehicles," *IEEE Transactions on Control Systems Technology*, Vol. 26, No. 3, 2017, pp. 939–953. doi:10.1109/TCST.2017.2699165

[59] Garg, K., and Panagou, D., "New Results on Finite-Time Stability: Geometric Conditions and Finite-Time Controllers," *2018 Annual American Control Conference*, IEEE Publ., Piscataway, NJ, 2018, pp. 442–447. doi:10.23919/ACC.2018.8431699

[60] Shen, Y., and Xia, X., "Semi-Global Finite-Time Observers for Nonlinear Systems," *Automatica*, Vol. 44, No. 12, 2008, pp. 3152–3156. doi:10.1016/j.automatica.2008.05.015

[61] Kartsatos, A. G., *Advanced Ordinary Differential Equations*, Mariner, Hindawi Publishing Co., Cairo, Egypt, 2005, Sec. 5.2.